SIAM J. Applied Dynamical Systems
Vol. 13, No. 1, pp. 1–46

Quasi-Periodic Frequency Analysis Using Averaging-Extrapolation Methods*

Alejandro Luque† and Jordi Villanueva‡

Abstract. We present a new approach to the numerical computation of the basic frequencies of a quasi-periodic signal. Although a complete toolkit for frequency analysis is presented, our methodology is better understood as a refinement process for any of the frequencies, provided we have a rough approximation of the frequency that we wish to compute. The cornerstone of this work is a recently developed method for the computation of Diophantine rotation numbers of circle diffeomorphisms, based on suitable averages of the iterates and Richardson extrapolation. This methodology was successfully extended to compute rotation numbers of quasi-periodic invariant curves of planar maps. In this paper, we address the case of a signal with an arbitrary number of frequencies. The most outstanding aspect of our approach is that frequencies can be calculated with high accuracy at a moderate computational cost, without simultaneously computing the Fourier representation of the signal. The method consists in the construction of a new quasi-periodic signal by appropriate averages of phase-shifted iterates of the original signal. This allows us to define a quasi-periodic orbit on the circle in such a way that the target frequency is the rotation frequency of the iterates. This orbit is well suited for the application of the aforementioned averaging-extrapolation methodology for computing rotation numbers. We illustrate the presented methodology with the study of the vicinity of the Lagrangian equilibrium points of the restricted three body problem (RTBP), and we consider the effect of additional planets using a multicircular model.

Key words. quasi-periodic frequency analysis, numerical approximation, invariant tori

AMS subject classifications. 34C15, 34C46, 37E45, 37J25, 37M10, 65Txx, 70K43

DOI. 10.1137/130920113

1. Introduction.

Invariant tori play a fundamental role in understanding the long-term behavior of dynamical systems. This is especially the case for Hamiltonian systems and also for exact symplectic maps, their discrete counterpart. If the Hamiltonian function is a small perturbation of an integrable Hamiltonian, the KAM theorem claims that, under generic assumptions, there are plenty of (maximal dimensional) invariant tori carrying quasi-periodic motion [1]. Invariant tori are also present far from integrability in the sense that they persist for larger values of the perturbation than predicted by KAM theory. There are other ways to generate quasi-periodic solutions apart from the close-to-integrable context. For example, if a system is forced periodically or quasi-periodically, fixed points, periodic orbits, and invariant tori inherit the frequencies of the perturbation [23, 38]. An analogous phenomenon takes place in the autonomous case, in connection with the excitation of elliptic

*Received by the editors May 7, 2013; accepted for publication (in revised form) by H. Osinga September 10, 2013; published electronically January 2, 2014. This work was partially supported by the Spanish MINECO-FEDER grants MTM2009-06973, MTM2012-31714, and MTM2012-32541 and the Catalan CUR-DIUE grant 2009SGR859.
http://www.siam.org/journals/siads/13-1/92011.html
†Departament de Matemàtica Aplicada i Anàlisi, Universitat de Barcelona, 08007 Barcelona, Spain (luque@maia.ub.es). This author's research was supported by the Juan de la Cierva Fellowship JCI-2010-06517.
‡Departament de Matemàtica Aplicada I, Universitat Politècnica de Catalunya, 08028 Barcelona, Spain (jordi.villanueva@upc.edu).

normal modes of linearly stable fixed points, periodic orbits, or lower dimensional invariant tori [10, 22]. These small oscillations generate new invariant tori. In addition, invariant tori are "effective barriers" to diffusion in phase space in the sense that trajectories close to a maximal dimensional torus or to a linearly stable lower dimensional one remain around it for a very long time [22, 33] (i.e., invariant tori are very "sticky"). These considerations lead quasi-periodic solutions to be the fundamental class of "stable solutions" in the Hamiltonian context. These solutions are relevant in applications to celestial mechanics, astrodynamics, molecular dynamics, and plasma-beam physics. Beyond the study of Hamiltonian systems and symplectic maps, existence of quasi-periodic solutions with stable behavior also occurs in other contexts, such as dissipative ordinary differential equations [3]. We refer the interested reader to [3, 4, 6, 38] and references therein for a wider picture of quasi-periodicity in dynamical systems.

Given an initial condition on a quasi-periodic torus, we can reconstruct this object from the corresponding orbit. If the dynamical system is defined by a map (discrete case), the iteration of this initial condition under the map defines a quasi-periodic signal. If the dynamical system is defined by a vector field (continuous case), this signal can be defined either by a stroboscopic section or by a Poincaré section.

The crucial issue to characterize quasi-periodic signals is to compute their frequencies. Indeed, the evolution of these frequencies along a family of trajectories allows us to understand the global behavior of the system, for example, by detecting resonances from the ratios between the computed frequencies. The regularity of the frequency map also provides information on the persistence of invariant tori. Moreover, the variation of the (local) frequencies with time is a dynamical indicator by which to measure diffusion and chaos [25].

The computation of frequencies and amplitudes of a signal is called quasi-periodic frequency analysis. We note that frequencies define a dense set of $\mathbb{R}$, although only a finite number of them may be independent. A vector of basic frequencies is any collection of independent frequencies. Frequencies are typically approximated by the peaks of the discrete Fourier transform (DFT) associated to a sample of points of the signal (see (30)). The size of the peak gives an approximation of the corresponding amplitude. This approximation is good up to errors of order $1/N$, where N is the number of points of the truncated signal. An important source of error is a phenomenon known as leakage. For periodic functions (the quasi-periodic case is similar), when the length T of the time interval spanned by the sample is not an integer multiple of the period, spurious frequencies appear in the DFT and the peaks are displaced. A procedure based on refined Fourier techniques to reduce leakage and improve this approximation was introduced in [25] (see also [26, 28]). This celebrated methodology introduces in the definition of the DFT a suitable window function, usually a power $p \geq 1$ of the so-called Hanning filter. After multiplying the quasi-periodic function by this window function, the derivatives of the new function vanish (up to order $2p-1$) at the endpoints of the interval. If the quasi-periodic function is smooth enough, then this new function can be extended outside $[0, T]$ as a periodic function of class $\mathcal{C}^{2p-1}$. This regularization has the effect of reducing the leakage phenomenon and allows for improving the resolution of the peaks corresponding to the dominant frequencies. After a frequency and its amplitude have been determined, this harmonic can be subtracted from the original signal, thus improving the computation of the remaining frequencies. This methodology has been successfully applied to

a wide set of problems (see, for example, [12, 27, 35] and references therein).

Among the improvements of this methodology, we highlight [13, 14]. The cornerstone of these papers is to refine both frequencies and amplitudes by a collocation method. Specifically, the signal is fitted to a generic Fourier expansion. After truncation of the series and discretization of the signal to a finite sample, the resulting system of nonlinear equations is solved simultaneously for both the frequencies and the Fourier coefficients (using the Newton method). The approximations of frequencies and amplitudes provided by the DFT are used as the initial guess for the solution of these equations.

There are other approaches to frequency analysis in the literature. For example, in [41] a method based on wavelets is presented, while [18] relies on the construction of sequences of orthogonal polynomials (frequencies are approximated by the zeros of these polynomials).

The methodology developed in the present paper assumes that we have a finite number of iterates of a quasi-periodic signal with Diophantine frequencies. We also suppose that the signal is analytic, although large enough differentiability suffices. Before discussing our approach to frequency analysis, let us outline some previous works that have laid the foundation of the method presented in this paper.

The cornerstone of our construction is a method introduced in [36] for computing Diophantine rotation numbers of circle diffeomorphisms. This method was justified under the assumption that the map is conjugate to a rigid rotation in a sufficiently smooth way. Basically, it consists in averaging the iterates of the map (actually its lift), together with Richardson extrapolation. In most of the cases, it is capable of computing the rotation number with high accuracy at low cost. We refer the reader to [8, 29, 37] for some works where this approach has been useful in dealing with problems related to circle maps.

The method of [36] was successfully extended in [30] to compute rotation numbers of quasi-periodic invariant curves of planar maps and, more generally, of quasi-periodic signals with one basic frequency ω. The methodology consists in building a new quasi-periodic signal having the same frequency. Any new iterate is defined by a weighted average of L consecutive phase-shifted iterates of the signal. Shifts are defined in terms of an approximation to the frequency of the signal (information on the amplitudes is not required). The purpose of these averages is to modify the Fourier coefficients of the signal so that the new one resembles as closely as possible a circle centered at the origin. For this reason, the construction is referred to as the "unfolding process." The goal is that the projection of the new signal onto the unit circle induces a circle diffeomorphism, defined by means of the correspondence between consecutive iterates. The rotation number of this map, which coincides with ω, can be obtained by the method of [36].

To ensure that the projection of the iterates generates a circle map, we can unfold the curve until we obtain a new one which is a graph over the argument. From the theoretical viewpoint, this achievement is possible if one has a sufficiently good approximation of the frequency and L is large enough. The complete unfolding of the signal can be quite expensive, but it turns out that the convergence of the curve to a circle can be accelerated by performing higher order averages and extrapolation (in analogy to the methodology of [36] for computing the rotation number). Moreover, in practice we do not need to unfold the curve completely. It suffices to unfold the curve removing only the main folds of the signal in such a way that the size of the remaining folds is small compared with the frequency ω. This is achieved with

a less expensive computational cost. Although the projection of the iterates onto the circle may not define a circle map, in general it defines a smooth quasi-periodic signal on the circle rotating with frequency ω (i.e., $\omega/2\pi$ is the averaged number of turns by iterate). It turns out that the method of [36] also works in this case for computing ω. The reason is that the key ingredient in [36] is not that the map is conjugate to a rigid rotation but that the iterates behave quasi-periodically on the circle. We extensively exploit this fact in the present work.

In this paper we arrange the methodology of [30] to deal with quasi-periodic signals depending on more than one basic frequency. A rough approximation[1] of the target frequency is used to unfold the signal, leading to a new quasi-periodic signal having the same frequencies as the original one. Under suitable conditions, the projection of the unfolded signal induces a quasi-periodically forced circle diffeomorphism. Now, the object projected onto the circle is not a curve but a strip (that can be viewed as a planar projection of a torus whose dimension is the number of basic frequencies of the signal). There is no general result ensuring that the dynamics of a given quasi-periodically forced circle map is conjugate to a rigid rotation (if this holds, conjugation depends quasi-periodically on the forcing frequencies). Existence of the conjugation is not guaranteed by any nonresonance condition or by the smoothness of the map (we refer the reader to [16, 17]). In the present context, if the projection truly defines such a map, then it is conjugate to a rotation by construction because the projected signal is already quasi-periodic. As noted before, in practice we need only a projected signal where the rotation frequency is the frequency that we want to compute, so we can apply the averaging-extrapolation methodology to refine it.

Let us summarize some features of the method. The computation of frequencies is carried out without simultaneously computing a Fourier representation of the signal. Fourier coefficients can be obtained a posteriori by slightly modifying the procedure for calculating the frequencies. Computation of frequencies is performed individually, so we can focus on one in particular. The same holds for the corresponding Fourier coefficient. The presented methodology is especially well suited if we are able to compute a large number of iterates of the signal with high precision. In most of the cases the method is capable of computing frequencies with great accuracy at a reasonable computational cost. As a conclusion, once we have an approximation to a particular frequency, the presented averaging-extrapolation approach can be viewed as a refinement process for it. Although this is not the ultimate purpose of this work, the proposed methodology can be arranged to get the required approximations.

From a theoretical viewpoint, the accuracy of the method is not constrained by the number of significant Fourier harmonics required to approximate the quasi-periodic signal or by the number of basic frequencies of the problem. Notice that after appropriate parameters have been selected to unfold the signal, the cost to calculate any new iterate is not conditioned by the accuracy that we want to achieve for the target frequency. By contrast, the accuracy expected by using the collocation procedure of [13, 14] is limited by the truncation order of the Fourier series. Indeed, if the problem has many basic frequencies or the Fourier coefficients do not decrease quickly enough, then performing high accuracy computation by fitting the Fourier expansion requires solving a system of large dimension. In the framework of the presented

[1]Sometimes this approximation is given by the context or by a preliminary study of the signal using a DFT-based method.

averaging-extrapolation construction, more precision can be obtained by computing more iterates of the signal (or, in the best-case scenario, by simply increasing the extrapolation order). This is done without increment of the memory cost and with a computational cost which is essentially linear on the number of computed iterates. If the signal is obtained by numerical integration of a vector field, the bottleneck in the computation time is the evaluation of the iterates and the cost of the method is almost negligible.

The paper is divided into two main parts. In section 2 we present the methodology for performing frequency analysis and related computations. This includes an informal exposition of the key ideas behind the "unfolding process." In section 3 we illustrate the presented methodology with the study of the vicinity of a Lagrangian equilibrium point of the restricted Sun–Jupiter–asteroid problem. We compute the frequencies for different sets of initial conditions to enhance some of the features of the methodology. We also consider a multicircular model where the effect of additional planets is taken into account. In Appendix A we pay attention to some algorithmic details so that the interested reader can implement this methodology, obtaining an efficient performance.

2. Description of the averaging-extrapolation methods.

In this section we present an averaging-extrapolation procedure for the computation of frequencies and amplitudes of a quasi-periodic signal. After introducing the problem in section 2.1, we summarize the main ideas behind our approach in section 2.2. We present our unfolding approach to single out a particular frequency in section 2.3. In section 2.4, we explain the averaging-extrapolation methodology to compute ("refine") this frequency. In section 2.5 we arrange this construction for the computation of the Fourier coefficients of the signal, while in section 2.6 we discuss how we can get approximations to the frequencies using the presented approach. In section 2.7 we test the methods by considering an example with known frequencies.

2.1. Setting of the problem.

In this section we set some basic notation and properties of quasi-periodic signals. We pay special attention to the construction of such signals in applications.

Definition 2.1. *Let $\mathbb{T}^r = \mathbb{R}^r/(2\pi\mathbb{Z})^r$ be the r-dimensional standard torus. We say that a complex sequence $\{z_n\}_{n\in\mathbb{Z}}$ is a quasi-periodic signal with frequency vector $\omega \in \mathbb{R}^r$ if there exists $\gamma : \mathbb{T}^r \to \mathbb{C}$ such that $z_n = \gamma(n\omega)$ $\forall n \in \mathbb{Z}$. If we denote the Fourier expansion of γ as*

$$\gamma(\theta) = \sum_{k\in\mathbb{Z}^r} \hat{\gamma}_k \mathrm{e}^{\mathrm{i}\langle k,\theta\rangle}, \qquad \hat{\gamma}_k = \frac{1}{(2\pi)^r} \int_{\mathbb{T}^r} \gamma(\theta)\mathrm{e}^{-\mathrm{i}\langle k,\theta\rangle} d\theta,$$

then we have the relation

$$z_n = \gamma(n\omega) = \sum_{k\in\mathbb{Z}^r} \hat{\gamma}_k \mathrm{e}^{\mathrm{i}n\langle k,\omega\rangle}. \tag{1}$$

In this paper we restrict the exposition to analytic signals. Analyticity of γ means that there exist positive constants ρ and M such that $|\hat{\gamma}_k| \le M\mathrm{e}^{-\rho|k|_1}$, where $|k|_1 := |k_1| + \cdots + |k_r|$.

We consider complex-valued analytic signals because this simplifies the presentation of the methods, even though large enough differentiability suffices (see [36] for details). The presented approach also works if $\{x_n\}$ is a real-valued quasi-periodic signal. The method itself

will turn it into a complex-valued one. If we have a vector-valued signal, $x_n = (x_n^1, \dots, x_n^l)$, then we have the chance to deal with one of the components or to build a complex signal from them (for example, $z_n = x_n^1$, $z_n = x_n^1 + \mathrm{i}x_{n+1}^1$, or $z_n = x_n^1 + \mathrm{i}x_n^2$). Note that it can be useful to define z_n so that it "turns" around the origin (or around any other point) with a rotation frequency that is close to that we wish to calculate. This can save many computations.

Remark 2.2. If ω verifies nonresonance conditions $\langle k, \omega\rangle + 2\pi m \neq 0$ for any $k \in \mathbb{Z}^r \setminus \{0\}$ and $m \in \mathbb{Z}$, then ω is called a vector of basic frequencies of the signal. If these nonresonance conditions are not met, then we can rewrite $\{z_n\}$ in terms of a lower number of frequencies. Besides nonresonance, we are going to assume that ω verifies Diophantine conditions of the form

$$|\mathrm{e}^{\mathrm{i}\langle k,\omega\rangle} - 1| \geq \frac{C}{|k|_1^\tau} \qquad \forall k \in \mathbb{Z}^r \setminus \{0\}, \tag{2}$$

for some $C, \tau > 0$. It is well known that if $\tau > r$, then the subset of $\omega \in \mathbb{R}^r$ for which conditions (2) do not hold, for any $C > 0$, has zero Lebesgue measure (see [6]).

Remark 2.3. The vector of basic frequencies $\omega \in \mathbb{R}^r$ is not univocally defined. If we perform the transformation $\omega \mapsto M\omega + 2\pi k$, with $k \in \mathbb{Z}^r$ and M an unimodular matrix, i.e., $M \in \mathbb{M}_{r\times r}(\mathbb{Z})$ with $\det(M) = \pm 1$, then we obtain an equivalent vector of basic frequencies. We have to be aware of this fact when performing the frequency analysis. On the one hand, such a property must be taken into account to correctly determine a set of basic frequencies. On the other hand, if the Fourier coefficient $\hat{\gamma}_{e_j}$ is small, then computing ω_j directly can be difficult. We have the chance to address its computation by dealing with another integer combination of basic frequencies $\langle k, \omega\rangle$, with $k_j \neq 0$, with a larger Fourier coefficient $\hat{\gamma}_k$.

Quasi-periodic signals like (1) are typically associated to a *discrete dynamical system*. This system can be defined by a map $F : U \subset \mathbb{R}^l \to \mathbb{R}^l$ or, more generally, by a quasi-periodically forced map $G : U \times \mathbb{T}^s \to \mathbb{R}^l \times \mathbb{T}^s$ of the form $G(x, \hat{\theta}) = (g(x, \hat{\theta}), \hat{\theta} + \hat{\omega})$, where $U \subset \mathbb{R}^l$ and $\hat{\omega} \in \mathbb{R}^s$. Let us suppose that $\gamma : \mathbb{T}^r \to \mathbb{R}^l$ is a parameterization of a quasi-periodic invariant torus of any of these maps. In the "autonomous case" we have $F(\gamma(\theta)) = \gamma(\theta + \omega)$. For quasi-periodically forced maps, the invariance condition is $g(\gamma(\theta), \hat{\theta}) = \gamma(\theta+\omega)$, where $\theta = (\widetilde{\theta}, \hat{\theta})$ and $\omega = (\widetilde{\omega}, \hat{\omega})$ (i.e., the torus inherits the frequencies of the forcing). If we take an initial condition on the torus, $x_0 = \gamma(\theta_0)$, for some $\theta_0 \in \mathbb{T}^r$, then $x_n = F^n(x_0)$ or $(x_n, n\hat{\omega}) = G^n(x_0, \hat{\theta}_0)$ defines a vector-valued quasi-periodic signal given by $x_n = \gamma(\omega n + \theta_0)$.

Let us also consider quasi-periodic functions of continuous variable $f : \mathbb{R} \to \mathbb{C}$, i.e., $f(t) = F(\widetilde{\omega}t)$, with $F : \mathbb{T}^r \to \mathbb{C}$ and $\widetilde{\omega} \in \mathbb{R}^r$. These are typically associated to a *continuous dynamical system*. We can introduce a (discrete-time) quasi-periodic signal as $z_n = f(nT)$ for a fixed $T > 0$. Then, $\{z_n\}$ has frequency vector $\omega = T\widetilde{\omega}$. In this situation we have to be aware of some facts due to the time discretization.

(a) Nonresonance conditions for a vector of basic frequencies of a continuous-time quasi-periodic signal are $\langle k, \widetilde{\omega}\rangle \neq 0\ \forall k \in \mathbb{Z}^r \setminus \{0\}$. To ensure that $T\widetilde{\omega}$ is a nonresonant frequency vector for the discretized signal, we need that $T \neq \frac{2\pi m}{\langle k,\widetilde{\omega}\rangle}$ for any $k \in \mathbb{Z}^r \setminus \{0\}$ and $m \in \mathbb{Z}$. It is equivalent to say that the $(r+1)$-dimensional vector $(\widetilde{\omega}, 2\pi/T)$ is a nonresonant frequency vector of a continuous-time quasi-periodic signal; i.e., we are adding an "artificial" frequency when performing the time discretization. In fact, an "exact resonance" between T and $\widetilde{\omega}$ is not a bad thing because then we are not

adding a new frequency due to the discretization (see Remark 2.4 for comments on time-dependent differential equations). Numerically, problems arise when we are close to a low-order resonance, i.e., $T \approx \frac{2\pi m}{\langle k,\widetilde{\omega}\rangle}$, with k and m not "too big." Then, we are going to have bad Diophantine conditions for ω (a small C in (2)). This is the worst situation for our methods. However, in the framework of this paper, the computation of $\widetilde{\omega}$ will follow from the prior knowledge of an approximate value $\widetilde{\omega}^0 \approx \widetilde{\omega}$. Then, we have the chance to ensure, numerically, that there are no low-order resonances between $\widetilde{\omega}^0$ and T.

(b) If $\omega \in \mathbb{R}^r$ is a vector of basic frequencies of the discretized signal, then we cannot always claim that ω/T is a vector of basic frequencies of the continuous-time signal. It turns out that we can select $\widetilde{\omega} = \omega/T + 2\pi m/T$ for some $m \in \mathbb{Z}^r$. Let $\widetilde{\omega}_0$ be an initial approximation to one of the components of $\widetilde{\omega}$, say, $\widetilde{\omega}_0 \approx \widetilde{\omega}_1 > 0$. Then, it is natural to select $T\widetilde{\omega}_0$ as initial approximation of a frequency of the discretized signal. If after application of our methodology we compute a refined value ω_1 such that $\omega_1 \approx T\widetilde{\omega}_1^0$, then it is quite natural that ω_1/T is a refined value for $\widetilde{\omega}_1$. However, we have to be careful with the "size" of the selected T. This is because our methodology is based on tracking how the argument of the discretized signal turns around the origin. Then, we must select T so that $T\widetilde{\omega}_1 < 2\pi$. Otherwise, what we compute is the value of $T\widetilde{\omega}_1$ minus the turns. See Remark 3.2 for additional comments.

Remark 2.4. A relevant case of a continuous quasi-periodic signal is a quasi-periodic invariant torus of an ordinary differential equation. Any trajectory on the torus defines a quasi-periodic function of continuous variable. Then, we introduce a discrete quasi-periodic signal as follows:

(a) If the equation is periodic or quasi-periodic in time, it is natural to perform stroboscopic sections. Indeed, in the periodic case one can select T as the period of the system. In the quasi-periodic case, if $\omega_1 > 0$ is a basic frequency of the differential equation, then it is natural to select $T = 2\pi/\omega_1$ (i.e., we are performing a Poincaré section by the angle associated to this frequency). This approach can also be used in the autonomous case in order to remove a frequency already known (for instance, a "dominant frequency," so that we "magnify" the contribution of the Fourier coefficients of the other ones). To do that, it is important to know it very accurately. Otherwise, instead of removing a frequency, we are replacing it by a close to resonant one (if ω_0 is this frequency and we take $T = 2\pi/\omega_1$, then we are adding the frequency $2\pi\omega_0/\omega_1$), which can lead the method to fail.

(b) In the autonomous case, one can define the discretized signal through a Poincaré section by a transversal hypersurface of the phase space. This has the advantage of removing a frequency of the quasi-periodic continuous-time signal instead of adding a new one.

2.2. Informal scheme of the main construction. In this section we outline the basic aspects of our approach to the computation of frequencies. We focus on the schematic exposition of the unfolding process, omitting details on the computation (refinement) of the frequencies and explanations on the methods to accelerate the convergence of the procedure.

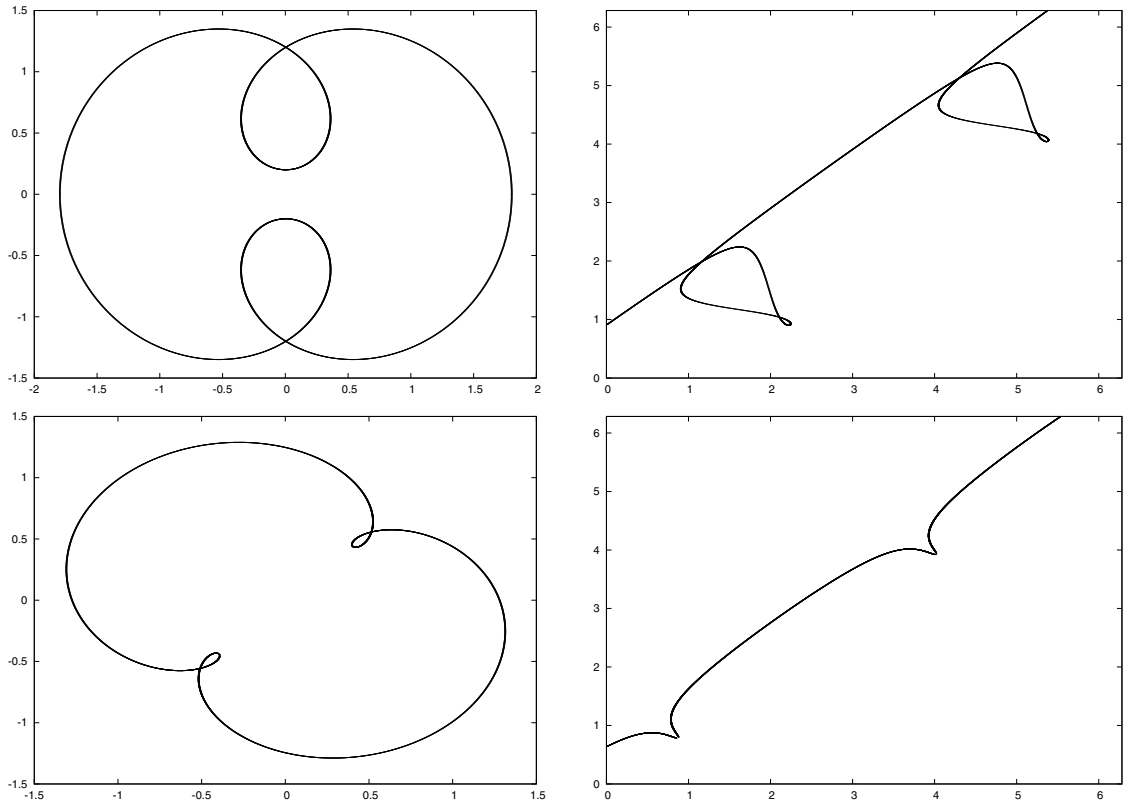

Figure 1. *The signal* (3) *for* $A = 1$, $B = 0.8$, $\omega_1 = (\sqrt{5}-1)\pi/8 \approx 0.4854$, *and* $\omega_2 = 2\omega_1$. *The top plots show the planar curve described by* (3) *and the correspondence* $\mathbb{R} \to \mathbb{R}$ *generated by a lift of the complex argument of the iterates. The bottom plots correspond to the unfolded signal* (6) *and its lift, with* $\omega_0 = \omega_1 + 0.1$ *and* $L = 4$. *As a matter of fact, the signal is completely unfolded for* $L = 5$, *and the lift becomes a graph.*

Let us consider a "toy example" given by the signal

$$z_n = A\mathrm{e}^{\mathrm{i}n\omega_1} + B\mathrm{e}^{\mathrm{i}n(\omega_1+\omega_2)} \tag{3}$$

for some $A, B \in \mathbb{C}$, with $\omega_j > 0$ and $\omega_j/2\pi \notin \mathbb{Q}$ for $j = 1, 2$. Note that if $\omega_1/\omega_2 \in \mathbb{Q}$, then (3) densely fills a planar curve (i.e., there is only one independent frequency). For general values of A and B this curve is noninjective and can have many folds (see Figure 1). If $\omega_1/\omega_2 \notin \mathbb{Q}$, then the signal can be viewed as a planar projection of a two-dimensional torus in $\mathbb{R}^3$. Throughout the exposition we concentrate on the computation of ω_1.

The simplest situation is when $B = 0$ and $A \neq 0$. Note that z_n belongs to the complex circle of radius $|A|$ centered at the origin. By means of the argument we can project this signal onto $\mathbb{T} = \mathbb{R}/2\pi\mathbb{Z}$. Then, the correspondence $z_n \mapsto z_{n+1}$ generates the rigid rotation $x \in \mathbb{T} \mapsto x + \omega_1 \in \mathbb{T}$, with rotation number $\omega_1/2\pi$. The fundamental point of our approach is that if $A \cdot B \neq 0$, but $|B/A|$ is small enough, then the projection of the signal onto the unit circle also generates an orbit with "rotation number" $\omega_1/2\pi$. Next we assume that $0 < |B/A| < 1$. In this case, we can find a simple expression for the dynamics of the argument. There exists

a periodic and analytic function $\varphi(\theta) = \arg(1 + (B/A)\mathrm{e}^{\mathrm{i}\theta})$ such that[2]

$$z_n = |A + B\mathrm{e}^{\mathrm{i}n\omega_2}|\mathrm{e}^{\mathrm{i}(n\omega_1 + \arg(A) + \varphi(n\omega_2))}, \tag{4}$$

so that the iterates $x_n = \arg(z_n)$ are given by

$$x_n = n\omega_1 + \arg(A) + \varphi(n\omega_2). \tag{5}$$

Now we consider two different situations:

- *We have a single independent frequency.* We assume that $\omega_2 = m\omega_1$ for some $m \in \mathbb{Z}$. If $|B/A|$ is small enough such that $|m\varphi'(\theta)| < 1\ \forall\theta \in \mathbb{T}$, then the correspondence $x_n \mapsto x_{n+1}$ generates a circle diffeomorphism $f : \mathbb{T} \to \mathbb{T}$. By construction, f is conjugate to the rigid rotation $x \mapsto x + \omega_1$. The conjugation is $\theta \mapsto \theta + \varphi(m\theta)$. In this case, we speak about a "projectable" curve or signal in the sense that the mere "projection" of the iterates onto $\mathbb{T}$ generates a circle diffeomorphism with the same frequency as the signal. We can evaluate a lift of f to $\mathbb{R}$ just by tracking how the iterates of the signal rotate around the origin (adding the accumulated turns to the argument of z_n). Indeed, formula (5) gives the expression of the iterates by the lift. As shown in section 2.4, the averaging-extrapolation methodology of [36] allows computing ω_1 from the iterates of the lifted signal.
- *We have two rationally independent frequencies.* If $B \neq 0$, the correspondence $x_n \mapsto x_{n+1}$ does not generate any circle map, but, since $|B/A| < 1$, it induces a quasi-periodically forced circle map with ω_2 as the frequency of the forcing. This map takes the form of a skew-product, $(\theta_1, \theta_2) \in \mathbb{T} \times \mathbb{T} \mapsto (f(\theta_1, \theta_2), \theta_2 + \omega_2) \in \mathbb{T} \times \mathbb{T}$. The transformation f is conjugate to the rigid rotation $x \mapsto x + \omega_1$ by a conjugation that depends quasi-periodically on θ_2, with frequency ω_2. This conjugation is $(\theta_1, \theta_2) \mapsto (\theta_1 + \varphi(\theta_2), \theta_2)$. If we compute the lift to $\mathbb{R}$ of the argument of the iterates $\{z_n\}$, it is also given by (5). Although now the right-hand side of (5) depends quasi-periodically on ω_2, we can compute ω_1 by averaging and extrapolation.

If $|B/A| \geq 1$, the discussions above are no longer true. Nevertheless, given an approximation ω_0 of ω_1, we can build a new quasi-periodic signal from (3) having the same frequencies, a slightly modified A, and a smaller B. In fact, given $L \in \mathbb{N}$, we introduce

$$z_n^{(L,\omega_0)} = \frac{1}{L}\sum_{m=n}^{L+n-1} z_m \mathrm{e}^{\mathrm{i}(n-m)\omega_0} = \frac{A}{L}\frac{1-\mathrm{e}^{\mathrm{i}(\omega_1-\omega_0)L}}{1-\mathrm{e}^{\mathrm{i}(\omega_1-\omega_0)}}\mathrm{e}^{\mathrm{i}n\omega_1} + \frac{B}{L}\frac{1-\mathrm{e}^{\mathrm{i}(\omega_1+\omega_2-\omega_0)L}}{1-\mathrm{e}^{\mathrm{i}(\omega_1+\omega_2-\omega_0)}}\mathrm{e}^{\mathrm{i}n(\omega_1+\omega_2)}. \tag{6}$$

Note that $z_n^{(L,\omega_0)}$ involves the sum of the L consecutive phase-shifted iterates $z_m\mathrm{e}^{-\mathrm{i}m\omega_0}$, $m = n, \ldots, L+n-1$. To understand the purpose of the construction in (6), we note that in the "limit case" $\omega_0 = \omega_1$ we get

$$z_n^{(L,\omega_1)} = A\mathrm{e}^{\mathrm{i}n\omega_1} + \frac{B}{L}\frac{1-\mathrm{e}^{\mathrm{i}\omega_2 L}}{1-\mathrm{e}^{\mathrm{i}\omega_2}}\mathrm{e}^{\mathrm{i}n(\omega_1+\omega_2)}. \tag{7}$$

Thus, for large enough values of L, the signal $z_n^{(L,\omega_1)}$ turns out to be "projectable" onto $\mathbb{T}$, giving rise to a circle map or to a quasi-periodically forced circle map, depending on the case,

[2] If $|B/A| > 1$, then the analytic continuation of $\varphi(\theta)$ is not periodic, but $\varphi(\theta + 2\pi) = \varphi(\theta) + 2\pi$.

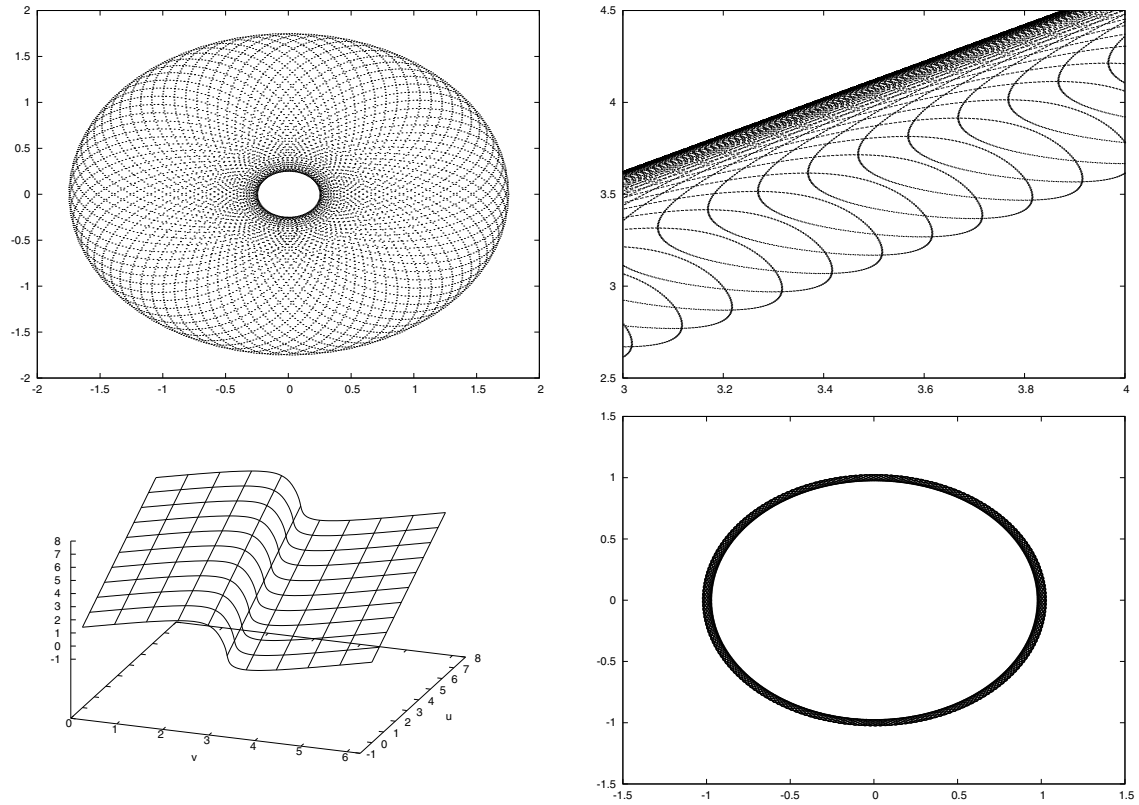

Figure 2. *The signal* (3) *for* $A = 1$, $B = 0.75$, $\omega_1 = (\sqrt{5}-1)\pi/8$, *and* $\omega_2 = (\sqrt{2}-1)\pi/4 \approx 0.3253$. *The top left plot shows how the dynamics densely fills the annulus that contains the orbit. The top right plot shows the correspondence* $\mathbb{R} \to \mathbb{R}$ *generated by a lift of the signal. This correspondence fills a strip in* $\mathbb{R}^2$ *(the plot shows how the dynamics organizes this strip). The bottom left plot shows the same lift, but now computed as* $\mathbb{R} \times \mathbb{T} \to \mathbb{R}$. *Synthetically, this lift is generated by the transformation* $(u, v) = (\arg(z_n), n\omega_2) \mapsto \arg(z_{n+1})$ *(i.e., v is the angle associated to* ω_2, *which is interpreted as a quasi-periodic forcing). The result looks like a smooth (but folded) surface. The bottom right plot shows the unfolded signal* (6) *for* $\omega_0 = \omega_1$ *(the exact frequency) and* $L = 20$. *The dynamics becomes a perturbation of a rotation of angle* ω_1 *on the unit circle.*

with rotation frequency ω_1. If $\omega_0 \approx \omega_1$ are close enough, then the behavior of $z_n^{(L,\omega_0)}$ is similar for "moderately large" values of L. In section 2.3 we show that if we have a generic quasi-periodic signal, with an arbitrary number of frequencies, then the same construction is useful in order to single out a particular frequency ω_1. This construction is illustrated in Figure 1 (ω_1 and ω_2 are dependent) and Figure 2 (ω_1 and ω_2 are independent). Due to the observed geometrical effect, we refer to this procedure as the unfolding of the signal.

We observe that if the signal is very folded (for example, if $|B/A|$ is very large in (3)), then it can be expensive to generate a projectable signal (even impossible if $|\omega_1 - \omega_0|$ is not extremely small). From the computational viewpoint, "expensive" means that we are forced to take large values of L in (6) in order to decrease the contribution of the Fourier coefficients different from that of $e^{in\omega_1}$. Fortunately, in applications it is not necessary to completely unfold the signal. Next, we try to clarify this assertion.

Let $\{z_n\}$ be a generic analytic and quasi-periodic signal with only one frequency $\omega_1 \in (0, 2\pi)$. Although the corresponding curve is nonprojectable, we can consider the dynamics of the argument along the iterates. Indeed, if $x_n = \arg(z_n)$, then the couples (x_n, x_{n+1}) generate a correspondence on the circle given by $x_n \in \mathbb{T} \mapsto x_{n+1} \in \mathbb{T}$. If we lift this correspondence to $\mathbb{R}$ along the whole curve, then we obtain a correspondence $\mathbb{R} \mapsto \mathbb{R}$. The lift describes how the argument of the iterates evolves along the origin, regardless of whether it moves forward or backward as a function of n (the lift must rise 2π for every turn of the signal). Although in general this lift is not a graph, it is natural to expect that it is given by an analytic curve. This is illustrated in Figure 1 for the signal in (3). By following the evolution of the lift along the iterates, we can define the rotation frequency $\bar{\omega}_1$ of the signal in a complete analogy to the rotation number of a circle map. Specifically, $\bar{\omega}_1/2\pi$ gives the average number of turns by iterate. The important thing is that not only is the mere definition $\bar{\omega}_1 = \lim_{n\to\infty}(x_n - x_0)/n$ valid in this case, but the averaging-extrapolation procedure of [36] works as well for accelerating the convergence to $\bar{\omega}_1$.

We note that $\bar{\omega}_1$ is not necessarily related to any frequency of the signal. If we have a good enough approximation of ω_1, then we can unfold $\{z_n\}$ by means of (6) until we get a projectable signal $\{z_n^{(L,\omega_0)}\}$, giving rise to a circle map of frequency ω_1. Hence, we truly have $\bar{\omega}_1 = \omega_1$ for the new signal. Moreover, practice shows that removing the main folds suffices to set the target frequency as a rotation frequency of this "partially unfolded signal," provided that the folds of the new signal are small compared with ω_1. These small folds are averaged out when computing the rotation frequency. Performing partial unfolding is computationally less demanding.

Let us summarize the discussion above for the signal (3) when $\omega_1/\omega_2 \in \mathbb{Q}$. The correspondence of $\mathbb{R}$ induced by the lift is analytic except when $|A| = |B|$. If $\omega_2 = m\omega_1$, then the condition $|m\varphi'| < 1$ in (5) ensures that the signal is projectable. In general, to ensure that the rotation frequency around the origin is ω_1, we need the weaker condition $|B/A| < 1$. This is enough for our purposes. When $|B/A| > 1$ the rotation frequency is $\omega_1 + \omega_2$. The unfolding method defines a new signal having the same frequency but with a smaller value of B.

For a quasi-periodic signal $\{z_n\}$ with many basic frequencies, $\omega \in \mathbb{R}^r$, the picture is very similar. Let ω_0 be a numerical approximation to one of the frequencies, say, $\omega_0 \approx \omega_1$. Assume that using (6) we can (partially) unfold the signal so that ω_1 is the rotation frequency around the origin of $\{z_n^{(L,\omega_0)}\}$. Then, the lift to $\mathbb{R}$ of the dynamics of the argument of $\{z_n^{(L,\omega_0)}\}$ generates a quasi-periodically forced correspondence of $\mathbb{R}$. The frequencies of the forcing are the $r-1$ remaining components of ω. We expect this lift to be given by an analytic expression in $\theta \in \mathbb{T}^r$, where θ are the angle variables of the torus that parameterizes the quasi-periodic signal (see Definition 2.1). Then, the methodology of [36] is well suited for computing ω_1 from the iterates of this lift.

Remark 2.5. To plot the lifts of these signals (Figures 1 and 2) we display the couples (x_n, x_{n+1}), where $x_n = \arg(z_n)$. We must take suitable determinations of the arguments (defined modulus 2π) in order to achieve the usual translation properties of the lift. As we have an explicit expression for the quasi-periodic signal (3), we can define $Z(\theta_1, \theta_2) = Ae^{i\theta_1} + Be^{i(\theta_1+\theta_2)}$ so that $z_n = Z(n\omega_1, n\omega_2)$. This allows using a continuous variable $t \in \mathbb{R}$ instead of the discrete one n, so that the plots can be made in terms of $z(t) = Z(\omega_1 t, \omega_2 t)$.

Then, the lift can be parameterized as $t \mapsto (x(t), x(t+1))$, where $x(t) = \arg(z(t))$. This corresponds to taking the closure of the lift computed only for the discrete iterates z_n.

2.3. Unfolding of the signal to isolate a frequency. In this section we describe in detail the unfolding process of a quasi-periodic signal that we have outlined in section 2.2. The goal is to build a new signal having the target frequency as a rotation frequency around the origin. This allows computing this particular frequency, with high accuracy, by the methodology of section 2.4. As we discussed in the introduction, the presented construction is an adaptation of the approach of [30].

This section is organized as follows. In section 2.3.1 we present the basic features of the unfolding process. This introduces a new quasi-periodic signal by a weighted average, inspired in the DFT, of some consecutive iterates. Under appropriate conditions, the convergence rate is of $\mathcal{O}(1/L)$, where L is the number of iterates involved in the average. In sections 2.3.2 and 2.3.3 we present higher-order averages that accelerate the convergence of the unfolding process up to orders $\mathcal{O}(1/L^2)$ and $\mathcal{O}(1/L^p)$, respectively.

2.3.1. First order unfolding. Here we present the fundamental method to unfold a quasi-periodic signal. The cornerstone is the following construction.

Definition 2.6. *Let $\{z_n\}_{n\in\mathbb{Z}}$ be an analytic complex-valued quasi-periodic signal as in Definition 2.1. We assume that the frequency vector $\omega \in \mathbb{R}^r$ verifies Diophantine conditions (2). For any $\omega_0 \in \mathbb{R}$ and $L \in \mathbb{N}$, we define the following iterates:*

$$z_n^{(L,\omega_0)} = \frac{1}{L}\sum_{m=n}^{L+n-1} z_m \mathrm{e}^{\mathrm{i}(n-m)\omega_0}. \tag{8}$$

It is easy to verify that for most[3] values of ω_0, the sequence $\{z_n^{(L,\omega_0)}\}_{n\in\mathbb{Z}}$ is a quasi-periodic signal with the same frequency vector ω. Indeed,

$$z_n^{(L,\omega_0)} = \gamma^{(L,\omega_0)}(n\omega) = \sum_{k\in\mathbb{Z}^r} \hat{\gamma}_k^{(L,\omega_0)} \mathrm{e}^{\mathrm{i}n\langle k,\omega\rangle}, \tag{9}$$

where the new Fourier coefficients are

$$\hat{\gamma}_k^{(L,\omega_0)} = \frac{\hat{\gamma}_k}{L}\sum_{m=n}^{L+n-1} \mathrm{e}^{\mathrm{i}(m-n)(\langle k,\omega\rangle-\omega_0)} = \frac{\hat{\gamma}_k}{L}\frac{1-\mathrm{e}^{\mathrm{i}L(\langle k,\omega\rangle-\omega_0)}}{1-\mathrm{e}^{\mathrm{i}(\langle k,\omega\rangle-\omega_0)}}. \tag{10}$$

Assume that ω_0 is one of the frequencies of the signal, say, $\omega_0 = \omega_1$. Omitting the dependence on ω_0, we write $z_n^{(L)} = z_n^{(L,\omega_1)}$. Then, expression (10) takes the form (compare with (7))

$$z_n^{(L)} = \sum_{k\in\mathbb{Z}^r} \hat{\gamma}_k^{(L)} \mathrm{e}^{\mathrm{i}n\langle k,\omega\rangle}, \quad \hat{\gamma}_{e_1}^{(L)} = \hat{\gamma}_{e_1}, \quad \hat{\gamma}_k^{(L)} = \frac{\hat{\gamma}_k}{L}\frac{1-\mathrm{e}^{\mathrm{i}L(\langle k,\omega\rangle-\omega_1)}}{1-\mathrm{e}^{\mathrm{i}(\langle k,\omega\rangle-\omega_1)}} \quad \text{for } k \neq e_1.$$

[3]The set of values of ω_0 for which $z_n^{(L,\omega_0)}$ is not quasi-periodic has zero Lebesgue measure. This theoretical situation plays no role in this work.

Since the signal is analytic and ω Diophantine, then $\hat{\gamma}_k^{(L)} = \mathcal{O}(\mathrm{e}^{-\rho|k|_1}|k-e_1|_1^{\tau}/L)$ if $k \neq e_1$. Consequently, for large enough values of L, the "unfolded signal" $\{z_n^{(L)}\}$ becomes a quasi-periodic perturbation of a planar rotation of angle ω_1. Indeed, provided that $\hat{\gamma}_{e_1} \neq 0$,

$$z_n^{(L)} = \hat{\gamma}_{e_1}\mathrm{e}^{\mathrm{i}n\omega_1}(1+\Gamma^{(L)}(n\omega)), \tag{11}$$

where $\Gamma^{(L)} : \mathbb{T}^r \to \mathbb{C}$ is analytic and $\Gamma^{(L)} = \mathcal{O}(1/L)$. We consider the projection of this orbit onto the circle $\mathbb{T} = \mathbb{R}/2\pi\mathbb{Z}$ through the argument

$$\begin{array}{ccc} \mathbb{C} & \longrightarrow & \mathbb{T}, \\ z_n^{(L)} & \longmapsto & x_n^{(L)} = \arg(z_n^{(L)}). \end{array} \tag{12}$$

If $\Gamma^{(L)}$ is small enough, then this projection introduces a quasi-periodic signal $\{x_n^{(L)}\}$ on $\mathbb{T}$ in such a way that the target frequency ω_1 is the rotation frequency of the iterates. Specifically, by using polar coordinates we can write

$$z_n^{(L)} = |\hat{\gamma}_{e_1}| \cdot |1+\Gamma^{(L)}(n\omega)|\mathrm{e}^{\mathrm{i}(n\omega_1+\phi^{(L)}(n\omega))},$$

where $\phi^{(L)} : \mathbb{T}^r \to \mathbb{R}$ is an analytic function, with $\phi^{(L)} = \mathcal{O}(1/L)$. Then $\{x_n^{(L)}\}$ is defined by taking modulo 2π on the expression

$$x_n^{(L)} = n\omega_1 + \phi^{(L)}(n\omega). \tag{13}$$

The cornerstone of the averaging-extrapolation method of section 2.4 for computing ω_1 is that (13) gives the lift to $\mathbb{R}$ of $\arg(z_n^{(L)})$.

Remark 2.7. Let us suppose that $\phi^{(L)}$ is small enough such that $\Psi(\theta) = (\theta_1+\phi^{(L)}(\theta), \hat{\theta})$ is a change of variables of $\mathbb{T}^r$, where $\theta = (\theta_1, \hat{\theta})$. Then, the correspondence $x_n^{(L)} \mapsto x_{n+1}^{(L)}$ induces a quasi-periodically forced circle map, where the frequencies of the forcing are $\hat{\omega} = (\omega_2, \ldots, \omega_r)$. This map takes the form $F(\theta) = (f(\theta), \hat{\theta}+\hat{\omega})$, where f is defined through the relation

$$f(\theta_1+\phi^{(L)}(\theta)) = \theta_1 + \omega_1 + \phi^{(L)}(\theta+\omega).$$

Then, $x_{n+1}^{(L)} = f(x_n^{(L)}, n\hat{\omega})$. By construction, the dynamics of $x_n^{(L)}$ is conjugate to the rotation $x \mapsto x+\omega_1$, by a conjugation that depends quasi-periodically on $\hat{\theta}$. Specifically, $F \circ \Psi(\theta) = \Psi(\theta+\omega)$. If Ψ is not a change of variables, but expression (13) holds, then the dynamics of $x_n^{(L)}$ is only semiconjugate to a rotation. Although in this situation we do not have any kind of circle map, semiconjugation suffices for our purposes (regardless of the size of $\phi^{(L)}$).

A realistic setting is to suppose that we know only an approximation ω_0 of ω_1, say, $\omega_0 = \omega_1+\varepsilon$. If ε is small enough, then it is natural to expect that we can choose $L = L(\varepsilon)$ such that the projection (12) of the "unfolded" signal $z_n^{(L,\omega_0)}$ has behavior similar to that when $\omega_0 = \omega_1$. If we want an expression like (13) for $x_n^{(L,\omega_0)} = \arg(z_n^{(L,\omega_0)})$, then $L|\varepsilon|$ must be fairly small. This is required to ensure that $\hat{\gamma}_1^{(L,\omega_0)}$ in (10) remains close to $\hat{\gamma}_1$, while the other Fourier coefficients behave as $\mathcal{O}(1/L)$.

Remark 2.8. If $\varepsilon \neq 0$, then (2) does not provide lower bounds for the denominators of $\hat{\gamma}_k^{(L,\omega_0)}$ in (10). The behavior of these denominators varies depending on the particular value

of $\omega_0 = \omega_1 + \varepsilon$ (resonances define a dense set). However, if ε is small, it is unlikely to find obstructions due to resonances. Besides the fact that the set of values of ε for which we do not have Diophantine bounds has zero Lebesgue measure, we also have the following observation. If ε is small, we can guarantee Diophantine bounds such as

$$|1 - \mathrm{e}^{\mathrm{i}(\langle k,\omega\rangle - \omega_0)}| \geq \frac{C/2}{|k - e_1|_1^\tau}, \qquad k \in \mathbb{Z}^r \setminus \{e_1\}, \tag{14}$$

up to a very large value of $|k|_1$ (precisely, up to $\mathcal{O}(1/\varepsilon_0^{1/\tau})$). As the Fourier coefficients $\hat{\gamma}_k$ are exponentially small on $|k|_1$, this means that the contribution of the remaining part of the Fourier series is very small (exponentially small in ε), with independence of any Diophantine bound. We do not formalize this fact precisely, but we refer the reader to [21], where this idea is the keystone of the paper.

Among the drawbacks of the method are the obvious constraints of a signal having very low regularity[4] or having close-to-resonant frequencies (with a very small C in (2) and (14)). Another limitation is when the Fourier coefficient of the frequency that we want to compute is small, e.g., when the signal is generated by a dynamical system that contains a small quasi-periodic perturbation and we want to compute the frequencies of the perturbation. A similar scenario is the study of a frequency associated to small oscillations around a linearly stable quasi-periodic torus of a Hamiltonian system. In these cases, unfolding the signal to single out such a frequency can be very difficult or even impossible. This does not imply that the method always fails to compute a frequency with small amplitude, but a very good approximation to this frequency is needed to unfold the signal, and the cost of the unfolding can be quite expensive. Sometimes this constraint can be addressed by changing the target frequency (in the sense of Remark 2.3). As a general rule, to tackle this issue we can subtract from the original signal the Fourier polynomial associated to its "dominant frequencies" (assuming they have been already computed).

Remark 2.9. Even when the unfolding process is unsuccessful (perhaps L is not large enough or the first approximation to ω_1 is not good enough), in general the averaging-extrapolation methodology of section 2.4 applied to $x_n^{(L,\omega_0)}$ converges to a certain value $\bar{\omega}_1$ (usually with high accuracy). The issue is if $\bar{\omega}_1$ is a true frequency of the signal. Fortunately, if $\bar{\omega}_1$ is not a frequency, then it is easy to realize the mistake. This is discussed in Remark 2.19. Then, we must improve the unfolding process.

In the best-case scenario, the new signal $z_n^{(L,\omega_0)}$ tends to be a rotation with a convergence rate of $\mathcal{O}(1/L)$. This is the same speed that we have when computing the rotation number of a circle map by the definition. In general, this is not quite satisfactory in practice. The issue is that if a large L is required, then this increases the computational cost. At first glance, we can subtract the average of the signal as a simple (but useful) way to improve the unfolding process. In sections 2.3.2 and 2.3.3 we describe a systematic procedure to accelerate the convergence of the unfolding.

[4]Finite differentiability means that $\hat{\gamma}_k$ is $\mathcal{O}(1/|k|_1^p)$. We require a sufficiently large p to justify our approach. We refer the reader to [37] for an example where averaging-extrapolation methods have been arranged to address a problem with very low regularity.

2.3.2. Second order unfolding. To accelerate the unfolding we perform higher-order averages and Richardson extrapolation. We start introducing the second order averages.

Definition 2.10. *Under the same notation and hypotheses of Definition 2.6, we introduce the sequences*

$$\mathcal{Z}_n^{(L,\omega_0,2)} = \sum_{l=1}^{L}\sum_{m=n}^{l+n-1} z_m \mathrm{e}^{-\mathrm{i}m\omega_0}, \qquad \widetilde{\mathcal{Z}}_n^{(L,\omega_0,2)} = \left(\frac{2}{L(L+1)}\mathcal{Z}_n^{(L,\omega_0,2)}\right)\mathrm{e}^{\mathrm{i}n\omega_0}. \tag{15}$$

Then, we define the following iterates:

$$z_n^{(2L,\omega_0,2)} = 2\widetilde{\mathcal{Z}}_n^{(2L,\omega_0,2)} - \widetilde{\mathcal{Z}}_n^{(L,\omega_0,2)}. \tag{16}$$

For most values of ω_0, the signal $\{z_n^{(2L,\omega_0,2)}\}_{n\in\mathbb{Z}}$ is quasi-periodic with frequency vector ω. As before, the limit case $\omega_0 = \omega_1$ is useful in illustrating the properties of the new iterates. Then, we write $\mathcal{Z}_n^{(L)} = \mathcal{Z}_n^{(L,\omega_1,2)}$ and compute

$$\begin{aligned}\mathcal{Z}_n^{(L)} &= \sum_{l=1}^{L}\sum_{m=n}^{l+n-1}\sum_{k\in\mathbb{Z}^r}\hat{\gamma}_k \mathrm{e}^{\mathrm{i}(m-n)(\langle k,\omega\rangle-\omega_1)}\\ &= \frac{L(L+1)}{2}\hat{\gamma}_{e_1} + L\sum_{k\neq e_1}\hat{\gamma}_k\frac{\mathrm{e}^{\mathrm{i}n(\langle k,\omega\rangle-\omega_1)}}{1-\mathrm{e}^{\mathrm{i}(\langle k,\omega\rangle-\omega_1)}} - \sum_{k\neq e_1}\hat{\gamma}_k\frac{1-\mathrm{e}^{\mathrm{i}L(\langle k,\omega\rangle-\omega_1)}}{(1-\mathrm{e}^{\mathrm{i}(\langle k,\omega\rangle-\omega_1)})^2}\mathrm{e}^{\mathrm{i}(n+1)(\langle k,\omega\rangle-\omega_1)}.\end{aligned}$$

Consequently,

$$\widetilde{\mathcal{Z}}_n^{(L)} = \hat{\gamma}_{e_1}\mathrm{e}^{\mathrm{i}n\omega_1} + \frac{2}{L+1}\mathcal{A}_1(n\omega) + \frac{2}{L(L+1)}\mathcal{E}_2(n\omega),$$

where $\mathcal{A}_1(n\omega)$ and $\mathcal{E}_2(n\omega)$ are quasi-periodic (and hence bounded) expressions. Note that if $\hat{\gamma}_{e_1} \neq 0$, the new iterates are given by

$$z_n^{(2L,\omega_1,2)} = \hat{\gamma}_{e_1}\mathrm{e}^{\mathrm{i}n\omega_1}(1+\Gamma^{(2L,\omega_1,2)}(n\omega)),$$

where $\Gamma^{(2L,\omega_1,2)} : \mathbb{T}^r \to \mathbb{C}$ verifies $\Gamma^{(2L,\omega_1,2)} = \mathcal{O}(1/L^2)$. Then, as done in (11), we can construct a quasi-periodic signal $\{x_n^{(2L,\omega_1,2)}\}_{n\in\mathbb{Z}}$ on $\mathbb{T}$, but now with a smaller perturbation of the rotation. As we show in Proposition 2.12, if $\omega_0 \approx \omega_1$, we have a similar scenario, at least for L not too large.

Besides motivating the reader, there are several reasons to introduce second order unfolding ($p = 2$) separately from the general case $p > 1$. On the one hand, in general the asymptotic rate $\mathcal{O}(1/L^2)$ gives a sufficiently good performance. On the other hand, we note that this asymptotic speed is secured only when $\omega_0 = \omega_1$. Hence, any discrepancy between ω_0 and our target frequency is propagated through the unfolding process. The potential disturbance of this discrepancy increases with the extrapolation order. Finally, note that for $p = 2$ we have explicit formulae (15) and (16) for any general value of L. In higher-order extrapolations we choose L as powers of 2 in order to obtain simple extrapolation coefficients.

2.3.3. Unfolding of order p. We introduce the following higher-order averages that extend Definitions 2.6 and 2.10 to any $p \in \mathbb{N}$.

Definition 2.11. *Under the same notation and hypotheses of Definition 2.6, we introduce the recursive sums*

$$\mathcal{Z}_n^{(L,\omega_0,1)} = \sum_{m=n}^{L+n-1} z_m \mathrm{e}^{-\mathrm{i}m\omega_0}, \qquad \mathcal{Z}_n^{(L,\omega_0,p)} = \sum_{l=1}^{L} \mathcal{Z}_n^{(l,\omega_0,p-1)}, \quad p \geq 2, \tag{17}$$

and the averaged sums of order p

$$\widetilde{\mathcal{Z}}_n^{(L,\omega_0,p)} = \left[\binom{N+p-1}{p}^{-1} \mathcal{Z}_n^{(L,\omega_0,p)} \right] \mathrm{e}^{\mathrm{i}n\omega_0}. \tag{18}$$

We take fixed values of $p \geq 1$ and $q \geq p$, and we define the new sequence

$$z_n^{(2^q,\omega_0,p)} = \sum_{j=0}^{p-1} c_j^{(p-1)} \widetilde{\mathcal{Z}}_n^{(L_j,\omega_0,p)}, \tag{19}$$

where $L_j = 2^{q-p+j+1}$ and the (extrapolation) coefficients $c_j^{(m)}$ are given by

$$c_j^{(m)} = (-1)^{m-j} \frac{2^{j(j+1)/2}}{\delta(j)\delta(m-j)}, \quad \delta(n) = (2^n-1)(2^{n-1}-1)\cdots(2^1-1), \quad \delta(0) = 1. \tag{20}$$

Sequence $\{z_n^{(2^q,\omega_0,p)}\}_{n\in\mathbb{Z}}$ gives an unfolding of order p of $\{z_n\}_{n\in\mathbb{Z}}$ computed from the approximate frequency ω_0. As before, for most values of ω_0, the new signal is quasi-periodic with frequency vector ω. Following [30, 36], we select L_j as powers of 2 in order to give explicit formulae for the extrapolation coefficients. Note that the important requirement for performing the extrapolation is that the values of L_j in (19) behave geometrically in j, so other choices can be made. To define $z_n^{(2^q,\omega_0,p)}$ we are using $L = 2^q$ consecutive iterates z_l, for $l \in \{n, \ldots, n+L-1\}$. As discussed in Proposition 2.12, if ω_0 is close enough to a particular frequency ω_1 and $L|\omega_0 - \omega_1|$ is fairly small, then $z_n^{(2^q,\omega_0,p)}$ is a perturbation of order $\mathcal{O}(1/L^p) = \mathcal{O}(2^{-pq})$ of a rotation of angle ω_1.

Proposition 2.12. *Assume the same notation and hypotheses of Definition 2.6, and suppose that ω_0 satisfies the Diophantine bounds in (14) $\forall k \in \mathbb{Z}^r \setminus \{e_1\}$. Then, there exists an analytic function $\gamma^{(2^q,\omega_0,p)} : \mathbb{T}^r \to \mathbb{C}$ such that the sequence $z_n^{(2^q,\omega_0,p)}$ introduced in Definition 2.11 can be written as $z_n^{(2^q,\omega_0,p)} = \gamma^{(2^q,\omega_0,p)}(n\omega)$. For every p we have*

$$|z_n^{(2^q,\omega_0,p)} - \hat{\gamma}_{e_1}^{(2^q,\omega_0,p)} \mathrm{e}^{\mathrm{i}n\omega_1}| = \mathcal{O}(2^{-pq}) \qquad \forall n \in \mathbb{Z}. \tag{21}$$

Moreover, the Fourier coefficient $\hat{\gamma}_{e_1}^{(2^q,\omega_0,p)}$ verifies $\lim_{\omega_0\to\omega_1} \hat{\gamma}^{(2^q,\omega_0,p)} = \hat{\gamma}_{e_1}$. This limit is uniform on q provided that $2^q|\omega_1 - \omega_0| \to 0$.

Proof. This result is a straightforward adaptation of Proposition 2.18 in [30], which essentially follows ideas introduced in [36]. For this reason, we focus on the computational details of the proof, omitting some technical aspects. We are referring to the quasi-periodic

expressions $\{\mathcal{A}_l^{(\omega_0,p)}\}_{l=1,\dots,p-1}$ and $\mathcal{E}^{(L,\omega_0,p)}$, which are convergent and bounded by a constant c_p (independent of L). By taking into account (14) and the analyticity assumptions on the signal, these claims are clear to any reader familiar with estimates on solutions of small divisor equations. For more details, see [36].

To simplify the notation we set $\varepsilon = \omega_1 - \omega_0$. The cornerstone of the proof is the following expressions, which can be easily obtained by induction:

$$\mathcal{Z}_n^{(L,\omega_0,p)} = \Delta^{(L,\omega_0,p)} \mathrm{e}^{\mathrm{i}n\varepsilon} + \left(\sum_{l=1}^{p-1} \binom{L+l-1}{l} \mathcal{A}_l^{(\omega_0,p)}(n\omega) + \mathcal{E}^{(L,\omega_0,p)}(n\omega) \right) \mathrm{e}^{-\mathrm{i}n\omega_0},$$

$$\widetilde{\mathcal{Z}}_n^{(L,\omega_0,p)} = \widetilde{\Delta}^{(L,\omega_0,p)} \mathrm{e}^{\mathrm{i}n\omega_1} + \sum_{l=1}^{p-1} \frac{(p-l+1)\cdots p\, \mathcal{A}_l^{(\omega_0,p)}(n\omega)}{(L+p-l)\cdots(L+p-1)} + \frac{p!\, \mathcal{E}^{(L,\omega_0,p)}(n\omega)}{L\cdots(L+p-1)},$$

where

$$\mathcal{A}_l^{(\omega_0,p)}(n\omega) = (-1)^{l+1} \sum_{k\neq e_1} \hat{\gamma}_k \frac{\mathrm{e}^{\mathrm{i}(l-1)(\langle k,\omega\rangle-\omega_0)}}{(1-\mathrm{e}^{\mathrm{i}(\langle k,\omega\rangle-\omega_0)})^l} \mathrm{e}^{\mathrm{i}n\langle k,\omega\rangle},$$

$$\mathcal{E}^{(L,\omega_0,p)}(n\omega) = (-1)^{p+1} \sum_{k\neq e_1} \hat{\gamma}_k \frac{\mathrm{e}^{\mathrm{i}(p-1)(\langle k,\omega\rangle-\omega_0)}(1-\mathrm{e}^{\mathrm{i}L(\langle k,\omega\rangle-\omega_0)})}{(1-\mathrm{e}^{\mathrm{i}(\langle k,\omega\rangle-\omega_0)})^p} \mathrm{e}^{\mathrm{i}n\langle k,\omega\rangle},$$

whereas $\Delta^{(L,\omega_0,p)}$ and $\widetilde{\Delta}^{(L,\omega_0,p)}$ are defined recursively by

$$\Delta^{(L,\omega_0,1)} = \hat{\gamma}_{e_1} \frac{1-\mathrm{e}^{\mathrm{i}\varepsilon L}}{1-\mathrm{e}^{\mathrm{i}\varepsilon}}, \quad \Delta^{(L,\omega_0,p)} = \sum_{l=1}^{L} \Delta^{(l,\omega_0,p-1)}, \quad \widetilde{\Delta}^{(L,\omega_0,p)} = \binom{L+p-1}{p}^{-1} \Delta^{(L,\omega_0,p)}.$$

It is not difficult to verify that $\lim_{\varepsilon\to 0} \widetilde{\Delta}^{(L,\omega_0,p)} = \hat{\gamma}_{e_1}$. We rewrite $\widetilde{\mathcal{Z}}_n^{(L,\omega_0,p)}$ as

$$\widetilde{\mathcal{Z}}_n^{(L,\omega_0,p)} = \widetilde{\Delta}^{(L,\omega_0,p)} \mathrm{e}^{\mathrm{i}n\omega_1} + \sum_{l=1}^{p-1} \frac{\widetilde{\mathcal{A}}_l^{(\omega_0,p)}(n\omega)}{L^l} + \widetilde{\mathcal{E}}^{(L,\omega_0,p)}(n\omega). \tag{22}$$

Note that the new function-coefficients $\{\widetilde{\mathcal{A}}_l^{(\omega_0,p)}\}_{l=1,\dots,p-1}$ $\widetilde{\mathcal{A}}_l^{(\omega_0,p)}$ are independent of L and that $\widetilde{\mathcal{E}}^{(L,\omega_0,p)}$ is of $\mathcal{O}(1/L^p)$, so expression (22) is well suited for Richardson extrapolation. A suitable combination of the averaged sums $\{\widetilde{\mathcal{Z}}_n^{(L_j,\omega_0,p)}\}_{j=0,\dots,p-1}$ with $L_j = 2^{q-p+j+1}$ allows removing the coefficients $\{\widetilde{\mathcal{A}}_l^{(\omega_0,p)}\}_{l=1,\dots,p-1}$. The resulting expression behaves in n like a rotation of angle ω_1 plus a quasi-periodic error of $\mathcal{O}(1/L_0^p)$.

To formalize this construction, we consider an arbitrary sequence $\{S_L\}_{L\geq 1}$ that satisfies

$$S_L = \alpha + \sum_{l=1}^{p-1} \frac{A_l}{L^l}. \tag{23}$$

In [30, 36] it was shown that $\alpha = \hat{\Theta}^{(p,q)}(\{S_L\})$, where the extrapolation operator $\hat{\Theta}^{(p,q)}$ is defined as

$$\hat{\Theta}^{(p,q)}(\{S_L\}) = \sum_{j=0}^{p-1} c_j^{(p-1)} S_{L_j}, \qquad L_j = 2^{q-p+j+1}, \tag{24}$$

and the coefficients $c_j^{(m)}$ are given in (20). Then, we use (24) for $S_L = \widetilde{\mathcal{Z}}_n^{(L,\omega_0,p)} - \widetilde{\Delta}^{(L,\omega_0,p)} \mathrm{e}^{\mathrm{i}n\omega_1} - \widetilde{\mathcal{E}}^{(L,\omega_0,p)}(n\omega)$ and $\alpha = 0$, thus obtaining

$$z_n^{(2^q,\omega_0,p)} = \gamma^{(2^q,\omega_0,p)}(n\omega) := \underbrace{\sum_{j=0}^{p-1} c_j^{(p-1)} \widetilde{\Delta}^{(L,\omega_0,p)}}_{\hat{\gamma}_{e_1}^{(2^q,\omega_0,p)}} \mathrm{e}^{\mathrm{i}n\omega_1} + \sum_{j=0}^{p-1} c_j^{(p-1)} \widetilde{\mathcal{E}}^{(L,\omega_0,p)}(n\omega).$$

Finally, bounds in (21) are straightforward, and $\lim_{\varepsilon\to 0} \hat{\gamma}_{e_1}^{(2^q,\omega_0,p)} = \hat{\gamma}_{e_1}$ follows from $\sum_{j=0}^{p-1} c_j^{(p-1)} = 1$. ∎

2.4. Computation of frequencies. In this section we sketch the method developed in [36] for computing Diophantine rotation numbers of circle diffeomorphisms. Other than for the sake of completeness, the main motivation for including this review in the paper is to show that the construction is well suited to deal with quasi-periodic signals on the circle depending on many frequencies. This methodology, applied to the unfolded signal constructed in section 2.3, constitutes the cornerstone of our approach to the computation of frequencies. We do not plan to perform a systematic presentation of the methodology or to discuss its full theoretical justification. For details we refer the reader to [36].

The starting point of the method is a quasi-periodic signal on $\mathbb{T}$ whose lift to $\mathbb{R}$ takes the form

$$x_n = n\omega_1 + \phi(\omega\theta) = n\omega_1 + \sum_{k\in\mathbb{Z}^r} \hat{\phi}_k \mathrm{e}^{\mathrm{i}\langle k,\omega\rangle}, \qquad n \in \mathbb{N}, \tag{25}$$

where $\phi : \mathbb{T}^r \to \mathbb{R}$. Our goal is to compute ω_1. Notice that we are not assuming that (25) is related to any kind of map or quasi-periodically forced map on the circle. In analogy with the definition of the rotation number of circle maps, we have that $\omega_1 = \lim_{n\to\infty}(x_n - x_0)/n$, for which we expect a convergence rate of $\mathcal{O}(1/n)$. Note that this rate is not satisfactory for practical purposes since it requires computing a tremendous number of iterates in order to reach a moderate tolerance. In a complete analogy with Definition 2.11, the key issue for accelerating the convergence speed of ω_1 is to introduce suitable recursive and averaged sums.

Definition 2.13. *Given a sequence $\{x_n\}_{n\geq 1}$, we introduce the recursive sums*

$$S_N^{(0)} = x_N, \qquad S_N^{(p)} = \sum_{n=1}^{N} S_n^{(p-1)}, \qquad N, p \geq 1,$$

and the averaged sums of order p

$$\widetilde{S}_N^{(p)} = \binom{N+p}{p+1}^{-1} S_N^{(p)}.$$

Note that the combinatorial numbers in the definition of $\widetilde{S}_N^{(p)}$ are not the same as those in the definition of $\widetilde{\mathcal{Z}}_n^{(L,\omega_0,p)}$ in (18). This is because the leading term of x_n in (25) is of $\mathcal{O}(n)$

while the term $\hat{\gamma}_1 \mathrm{e}^{\mathrm{i}n\omega_1}$ that we want to extrapolate from z_n in (1) is of $\mathcal{O}(1)$. This discrepancy between the "dominant orders" is also evident in the expressions of the corresponding extrapolation operators (compare (23) and (24) with (27)).

Proposition 2.14. *Let us consider a real-valued signal $\{x_n\}_{n\in\mathbb{N}}$ of the form (25). We assume that ϕ is analytic and that the vector $\omega \in \mathbb{R}^r$ verifies Diophantine conditions (2). Then, we have the following expression for the averaged sums of Definition 2.13:*

$$\widetilde{S}_N^{(p)} = \omega_1 + \sum_{l=1}^{p} \frac{\widetilde{A}_l^{(p)}(n\omega)}{N^l} + \widetilde{E}^{(N,p)}(n\omega), \qquad N \geq 1, \tag{26}$$

where $\{\widetilde{A}_l^{(p)}(n\omega)\}$ and $\widetilde{E}^{(N,p)}(n\omega)$ are analytic and quasi-periodic expressions, with $\widetilde{E}^{(N,p)} = \mathcal{O}(1/N^{p+1})$.

Furthermore, we consider fixed integer values $q \geq p \geq 1$, and we define the following extrapolation operator of order p, which involves $N = 2^q$ consecutive iterates of $\{x_n\}_{n\in\mathbb{N}}$:

$$\Theta^{(p,q)} = \sum_{j=0}^{p} c_j^{(p)} \widetilde{S}_{N_j}^{(p)}, \tag{27}$$

where $N_j = 2^{q-p+j}$ and the coefficients $c_j^{(p)}$ are given in (20). Then, we have

$$\omega_1 = \Theta^{(p,q)} + e(p,q), \tag{28}$$

where $e(p,q) = \mathcal{O}(1/N^{p+1}) = \mathcal{O}(2^{-(p+1)q})$.

We omit the proof of Proposition 2.14 because it follows the same reasoning as the proof of Proposition 2.12. As in Definition 2.11, we select N_j as powers of two.

Remark 2.15. Selecting appropriate values of p and q to extrapolate the frequency is independent of how the signal has been unfolded. The values of p and q in $\Theta^{(p,q)}$ in (27) have nothing to do with their counterparts in $z_n^{(2^q,\omega_0,p)}$ in (19).

Remark 2.16. If the signal comes from experimental data, then it is natural to assume that it contains some roundoff errors that behave in random way. Such a situation was discussed in [30], where the uncertainty coming from experimental data was simulated by adding to a quasi-periodic signal (with just one frequency) a normally distributed random error. The result was that the presented methodology still provides very accurate approximations to the frequency of the signal, significantly smaller than the size of the random component.

Remark 2.17. The methodology of [36] for computing rotation numbers was addressed in [29] to compute derivatives of the rotation number with respect to parameters. Although this issue is not discussed in this paper, this approach can be adapted to the framework of the frequency analysis.

2.5. Computation of amplitudes. In a very naive way, the unfolding construction presented in section 2.3 basically tries to extrapolate the Fourier harmonic corresponding to the "closest frequency" to ω_0. Once we have computed a refined value for the approximate frequency ω_0, we can adapt the construction to get a posteriori the corresponding amplitude by means of averaging and extrapolation. We emphasize that this procedure does not require any information on the remaining frequencies.

Proposition 2.18. *With the same notation and hypotheses of Definition 2.6, let $k^* \in \mathbb{Z}^r$ and $\omega^* = \langle k^*, \omega \rangle$ (i.e., ω^* is the combination of the basic frequencies $\omega \in \mathbb{R}^r$ associated to the Fourier coefficient $\hat{\gamma}_{k^*}$ in (1)). We introduce the following recursive and averaged sums for the quasi-periodic signal $\{z_n\}$, for any $N, p \geq 1$:*

$$\mathcal{F}_N^{(k^*,0)} = z_N \mathrm{e}^{-\mathrm{i}N\omega^*}, \quad \mathcal{F}_N^{(k^*,p)} = \sum_{n=1}^{N} \mathcal{F}_n^{(k^*,p-1)}, \quad \widetilde{\mathcal{F}}_N^{(k^*,p)} = \binom{N+p-1}{p}^{-1} \mathcal{F}_N^{(k^*,p)}.$$

Furthermore, given integer values $q \geq p \geq 1$, we define the following extrapolation operator of order p, which involves $N = 2^q$ consecutive iterates of $\{z_n\}$:

$$\Gamma^{(k^*,p,q)} = \sum_{j=0}^{p-1} c_j^{(p-1)} \widetilde{\mathcal{F}}_{L_j}^{(k^*,p)}, \tag{29}$$

where $L_j = 2^{q-p+j+1}$ and the coefficients $c_j^{(p-1)}$ are given in (20). Then, we have

$$\hat{\gamma}_{k^*} = \Gamma^{(k^*,p,q)} + e(k^*, p, q),$$

where $e(k^*, p, q) = \mathcal{O}(1/N^p) = \mathcal{O}(2^{-pq})$.

Proposition 2.18 follows by the same arguments as Propositions 2.12 and 2.14 (see [30] for the case of one basic frequency). Although this result is formulated in terms of a single amplitude, it can be performed simultaneously for multiple Fourier coefficients in the spirit of FFT strategies. This saves operations when computing the Fourier representation of the signal.

We take note of some problems that may arise when computing $\hat{\gamma}_{k^*}$ for large values of k^*. On the one hand, the smallness of $\hat{\gamma}_{k^*}$ makes it difficult to obtain a significant expression for it. On the other hand, the disturbing effect of the dominant Fourier coefficients of the signal is present along the averaging-extrapolation process. Although (29) provides a numerical value for $\hat{\gamma}_{k^*}$ with an error of $\mathcal{O}(2^{-pq})$, such a result follows after many cancellations between expressions of size larger than $\hat{\gamma}_{k^*}$. This leads to the loss of many significant digits. If an accurate Fourier representation of $\{z_n\}$ is needed, one can try to combine Proposition 2.18 with the collocation methods of [13, 14] already mentioned in the introduction. This allows us to refine amplitudes and frequencies by the Newton method. Furthermore, sometimes the iterates $\{z_n\}$ correspond to an initial condition giving an approximation of an invariant torus of a Hamiltonian system or symplectic map. In the literature there are "nonperturbative" KAM methods proving existence of quasi-periodic solutions close to a good-enough candidate (see, for example, [7, 15, 31]). Then, after computing the approximate frequencies and amplitudes for $\{z_n\}$, we can correct them by means of these KAM schemes.

In addition to the pure computation of the Fourier coefficients, the following remarks account for some interesting applications of Proposition 2.18.

Remark 2.19. As noted in Remark 2.9, if the unfolding is not performed correctly, it can happen that the refinement of a frequency (algorithm described in section 2.4) converges to a value $\bar{\omega}_1$ which is not a frequency of the original signal. Indeed, we can only claim that $\bar{\omega}_1$ is the rotation frequency around the origin of the partially unfolded signal. In general,

we can easily realize this failure due to a big discrepancy between the approximate frequency ω_0 and the computed value $\bar{\omega}_1$. A systematic way to check the correctness of $\bar{\omega}_1$ is to apply Proposition 2.18 with $\omega^* = \bar{\omega}_1$. If $\bar{\omega}_1$ is a true frequency, then we end up computing the corresponding Fourier coefficient. If $\bar{\omega}_1$ is not a frequency, we expect that the extrapolated amplitude tends to zero very quickly.

Remark 2.20. The simplest but perhaps most interesting case of Proposition 2.18 is for $k^* = 0$. Note that $\hat{\gamma}_0$ corresponds to the average of the quasi-periodic signal, which can be computed without any information on the frequencies. Let us observe that the computational cost of $\hat{\gamma}_0$ is fairly less expensive than that of any other Fourier coefficient (there is no trigonometric part involved in the computations). We have the following straightforward applications:

(a) Generically, $\hat{\gamma}_0$ is one of the largest Fourier coefficients of the signal. If we subtract $\hat{\gamma}_0$ from the signal, then we can improve the unfolding process.

(b) The study of the convergence of $\Gamma^{(0,p,q)}$ in (29) can be used as a fast indicator to decide if a given orbit is quasi-periodic or not before performing frequency analysis. Note that fast convergence does not always mean that the signal is quasi-periodic (for instance, this criterion also detects initial conditions belonging to the stable manifold of an invariant torus). Moreover, divergence of $\Gamma^{(0,p,q)}$ (including oscillatory behavior) or even slow convergence means that the signal is not quasi-periodic (or, at least, that it has bad Diophantine frequencies).

2.6. First approximation of frequencies. As explained in the introduction, the classical method to obtain approximations of the frequencies of a quasi-periodic signal is to look for the peaks of the modulus of its DFT.

The unfolding methodology presented in this paper requires approximations of the frequencies (but not of the corresponding amplitudes). Sometimes these approximations are given by the context, e.g., if we are in a neighborhood of an elliptic fixed point or carrying out continuation with respect to parameters of a quasi-periodic solution with known frequencies. In section 3 we study a (large) neighborhood of an elliptic equilibrium point of a Hamiltonian system, and we include quasi-periodic perturbations. In this case, one can perform a continuation process for the frequencies starting close to the equilibrium point. Otherwise, we can obtain approximations to the frequencies by a preliminary study of the signal by a DFT-based method (performed with low accuracy).

Additionally, we have the chance to adapt the unfolding methodology of section 2.3 in order to get such approximations. We outline this approach, which can be understood as an alternative to the use of filters in the DFT. We refer the reader to [30] for the case of a single frequency and for the accurate description of some implementation details.

Let us consider a quasi-periodic signal $\{z_n\}$. From a sample of L points we compute its DFT as a function of ω_0, given by the formula

$$\omega_0 \longmapsto \frac{1}{L}\sum_{m=0}^{L-1} z_m \mathrm{e}^{-\mathrm{i}m\omega_0}. \tag{30}$$

This expression coincides with the "zero iterate" $z_0^{(L,\omega_0)}$ of the unfolded signal (8) of order $p = 1$. We denote $Z^{(L,1)}(\omega_0) = |z_0^{(L,\omega_0)}|$ the modulus of (30). The classical approach to the

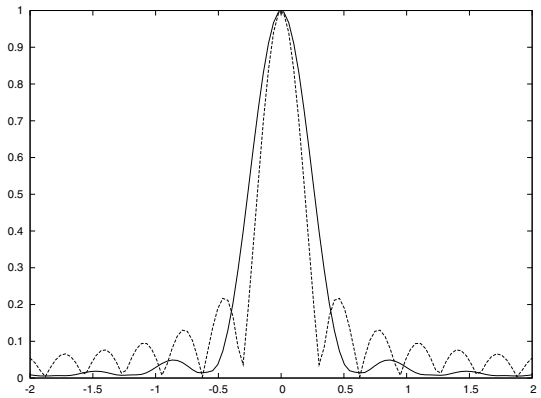

Figure 3. *Comparison between $Z_0^{(2L,2)}(\omega_0)$ (continuous graph) and $Z_0^{(2L,2)}(\omega_0)$ (discontinuous graph) for $L = 10$. We plot these functions in terms of $\omega_1 - \omega_0$, and so the desired local maximum is set at the origin.*

frequency analysis is based on the following observation. Assume for the moment that $\{z_n\}$ is a quasi-periodic signal consisting of a single Fourier harmonic, say, $z_n = \mathrm{e}^{\mathrm{i}n\omega_1}$. Then, the modulus of the DFT is given by

$$Z_0^{(L,1)}(\omega_0) = \frac{1}{L}\left|\frac{\sin(L(\omega_1-\omega_0)/2)}{\sin((\omega_1-\omega_0)/2)}\right|, \tag{31}$$

which has a local maximum at $\omega_0 = \omega_1$. If $\{z_n\}$ is a generic (but smooth enough) quasi-periodic signal, then the effect of the remaining Fourier harmonics on $Z^{(L,1)}(\omega_0)$ can be viewed as a perturbation of (31) around $\omega_0 = \omega_1$. This leads to a displacement of the maximum of $Z_0^{(L,1)}(\omega_0)$, which allows computing a "dominant" frequency ω_1 of $\{z_n\}$ with an accuracy of $\mathcal{O}(1/L)$. As we already summarized in the introduction, this displacement can be modulated by introducing suitable window functions in the DFT.

We propose a new approach to correct the DFT based on higher-order unfoldings. Let us concentrate on the case $p = 2$. We consider a sample of $2L$ points of $\{z_n\}$ and introduce $Z^{(2L,2)}(\omega_0) = |z_0^{(2L,\omega_0,2)}|$, where $z_0^{(2L,\omega_0,2)}$ is the zero iterate of the unfolded signal (see Definition 2.10). If $z_n = \mathrm{e}^{\mathrm{i}n\omega_1}$, then it is not difficult to realize that the corresponding function giving the modulus, namely, $Z_0^{(2L,2)}(\omega_0)$, also reaches a local maximum at $\omega_0 = \omega_1$. As shown in Figure 3, the resolution of this maximum for $Z_0^{(2L,2)}(\omega_0)$ is magnified with respect to $Z_0^{(2L,1)}(\omega_0)$ in the sense that the spurious peaks nearby are modulated by the unfolding. We recall that when $\omega_0 \approx \omega_1$ are close enough (see Proposition 2.12), then the unfolded signal "tends to" the planar rotation $\mathrm{e}^{\mathrm{i}n\omega_1}$ with a convergence rate of $\mathcal{O}(1/L^2)$ (see Proposition 2.12). This implies that we can determine a dominant frequency ω_1, up to an accuracy of $\mathcal{O}(1/L^2)$, from the study of $Z^{(2L,2)}(\omega_0)$. We can extend this construction up to an arbitrary order p by considering $Z^{(2^q,p)}(\omega_0) = |z_0^{(2^q,\omega_0,p)}|$ (see Definition 2.11). In this way, the theoretical resolution of the maximum improves up to $\mathcal{O}(2^{-pq})$ (see Proposition 2.12).

To built a refined methodology to detect frequencies based on the study of the maxima of $Z^{(2^q,p)}(\omega_0)$ is not the purpose of this work (this is the spirit of [25, 13]), although in this way we have the chance to implement a self-contained toolkit to perform frequency analysis. We

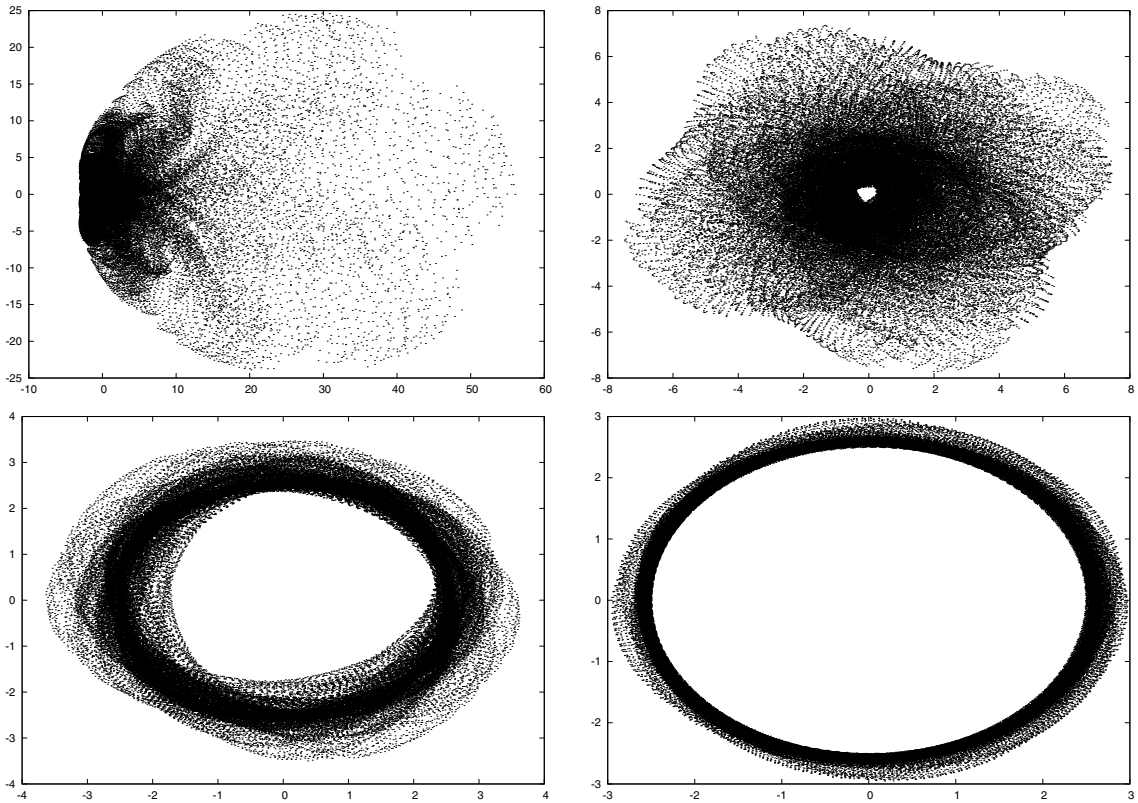

Figure 4. *We show 10^5 iterates of the quasi-periodic signal defined by (32) (top left plot) and the corresponding unfolded signals $\{z_n^{(L,\omega_1)}\}$ using $L = 8$ (top right plot), $L = 32$ (bottom left plot), and $L = 128$ (bottom right plot).*

remark that dealing with $Z^{(2^q,p)}(\omega_0)$ has some advantages with respect to introducing filters on the DFT, from the point of view of both dynamics and regularity. For example, if we introduce a Hanning filter on the DFT, then we are turning any analytic quasi-periodic signal into a periodic one, with a regularity that depends on the order of the filter. In this way, the Fourier coefficients of the filtered signal behave asymptotically as an inverse power of the order of the coefficient. By contrast, the unfolding procedure of this paper keeps both the analyticity and quasi-periodicity of the signal. In particular, we are not introducing spurious frequencies due to the length of the selected sample. Moreover, if $\omega_0 \approx \omega_1$, then we expect the contribution to $Z^{(2^q,p)}(\omega_0)$ of the high-order Fourier harmonics to be exponentially small with respect to the order.

2.7. Testing the method with a known quasi-periodic signal. In this section we test the performance of the presented methods in an example with known frequencies. Let us consider a quasi-periodic signal $z_n = \gamma(\omega n)$, with three independent frequencies, given by

$$\gamma(\theta_1,\theta_2,\theta_3) = \frac{\mathrm{e}^{\mathrm{i}\theta_1} + \mathrm{e}^{\mathrm{i}\theta_2} + \mathrm{e}^{\mathrm{i}\theta_3} + \mathrm{e}^{\mathrm{i}(\theta_1+\theta_2)} + \mathrm{e}^{\mathrm{i}(\theta_2+\theta_3)} + \mathrm{e}^{\mathrm{i}(\theta_1-\theta_3)} + \mathrm{e}^{3\mathrm{i}\theta_1}}{(1-\mu\cos(\theta_1))(1-\mu\cos(\theta_2))(1-\mu\cos(\theta_3))}, \tag{32}$$

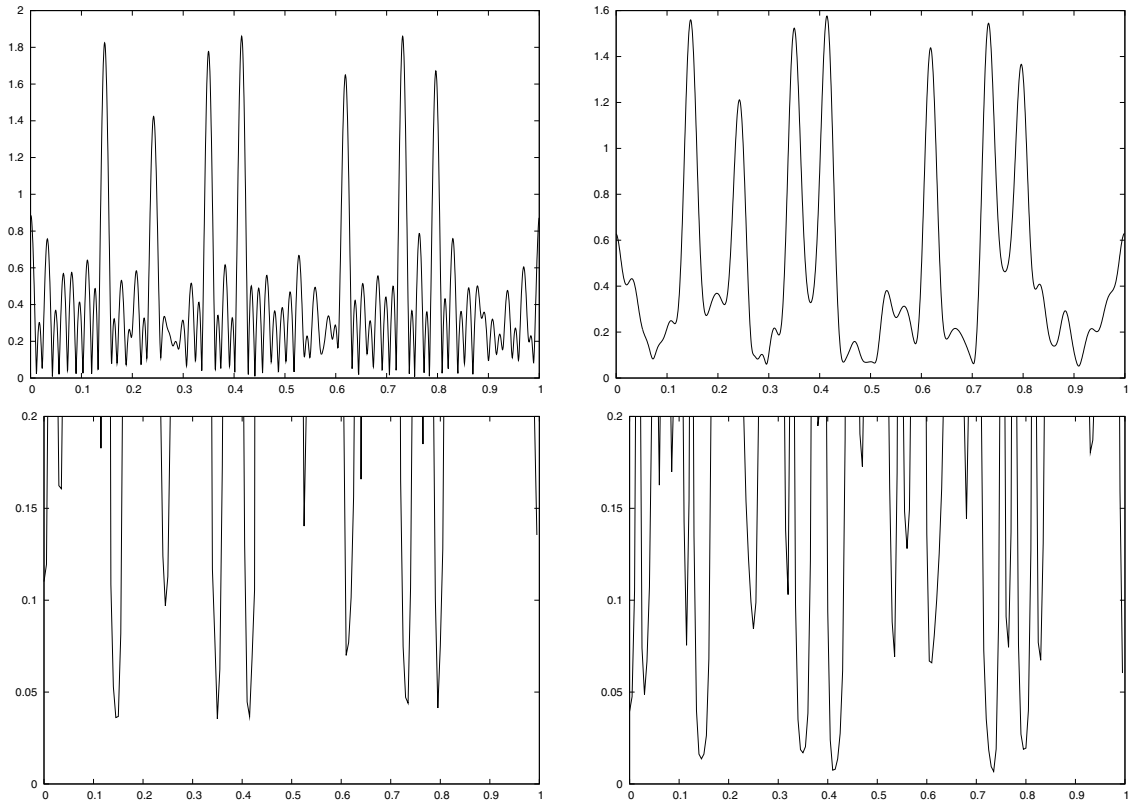

Figure 5. *Top: We plot* $\frac{\omega_0}{2\pi} \in [0,1] \mapsto Z^{(64,p)}(\omega_0)$ *for* $p = 1$ *(left plot) and* $p = 2$ *(right plot). Bottom: We plot the standard deviation of the radius for the first* 50000 *unfolded iterates* $z_n^{(2^6,\omega_0,p)}$ *as a function of* $\frac{\omega_0}{2\pi} \in [0,1]$ *for* $p = 1$ *(left plot) and* $p = 2$ *(right plot).*

where $\omega_1 = 2\pi(\sqrt{2}-1)$, $\omega_2 = 2\pi(\sqrt{3}-1)$, and $\omega_3 = \pi(\sqrt{5}-1)$. Taking $\mu \neq 0$ allows us to introduce infinitely many harmonics and to break the entire character of the signal. From the qualitative viewpoint, results do not depend on the particular value of $0 < \mu < 1$, so we take $\mu = 0.3$ in all the computations. Notice that if $\mu \to 1$, then the strip of analyticity of $\gamma(\theta)$ around $\theta \in \mathbb{T}^3$ collapses on the real torus. The reader interested in the behavior of averaging-extrapolation methods outside their domain of validity is referred to [8, 37].

Some iterates of (32) are shown in Figure 4. We also plot the corresponding first order unfolded signals $\{z_n^{(L,\omega_0)}\}$ (see Definition 2.6), computed in terms of the exact frequency $\omega_0 = \omega_1$ and for $L = 8, 32$, and 128. We observe how the cloud of points of the original signal, that fills up densely an open set of the plane, approaches (as L increases) a more organized distribution of points on an annulus.

Let us illustrate how we can obtain a first guess of the frequencies using the method presented in section 2.6. We assume for the moment that the iterates $\{z_n\}$ are known but that the frequencies of the signal are unknown. We must stress that here we are more interested in illustrating the observed phenomena rather than in describing an efficient and fast implementation of the algorithm. At the top of Figure 5 we show the function $\frac{\omega_0}{2\pi} \mapsto Z^{(L,p)}(\omega_0)$

for $p = 1$ (left plot) and $p = 2$ (right plot) using only $L = 64$ (in the plots frequencies are represented modulo 1 rather than modulo 2π). The main peaks observed are candidates for approximations of the frequencies of the signal. Observe that for $p = 2$ the number of spurious peaks is significantly reduced. For example, if we compute $Z^{(64,2)}(\omega_0)$ for a sample of 200 points $\frac{\omega_0}{2\pi} \in [0, 1]$ (with step 0.005), then the numerical approximations for the picks are easy to relate to combinations of the basic frequencies of (32). Indeed, $0.415 \simeq \frac{1}{2\pi}\omega_1$, $0.730 \simeq \frac{1}{2\pi}\omega_2$, and $0.620 \simeq \frac{1}{2\pi}\omega_3$. Other relevant peaks are, for example, $0.145 \simeq \frac{1}{2\pi}(\omega_1 + \omega_2)$, $0.24 \simeq \frac{1}{2\pi}3\omega_1$, $0.350 \simeq \frac{1}{2\pi}(\omega_2 + \omega_3)$, and $0.795 \simeq \frac{1}{2\pi}(\omega_1 - \omega_3)$.

We recall that $Z^{(L,p)}(\omega_0)$ gives the modulus of the zero unfolded iterate computed in terms of the approximate frequency ω_0. Hence, $Z^{(L,p)}(\omega_0)$ is useful in detecting approximations to the frequencies but does not show the dynamical features of the unfolding. Now, we illustrate the behavior of the unfolding process in connection with the peaks of $Z^{(64,p)}(\omega_0)$. The aim is to characterize the phenomenology displayed in Figure 4 in a systematic way.

For a given ω_0, we compute 50000 iterates of the unfolded signal $\{z_n^{(2^6,\omega_0,p)}\}$ (see Definition 2.11), and we estimate the distance to a circle around the origin by the standard deviation of its averaged radius. Results as function of $\frac{\omega_0}{2\pi} \in [0, 1]$ are shown at the bottom of Figure 5 for $p = 1$ (left plot) and $p = 2$ (right plot). In this way, we illustrate how the unfolded process is successful when ω_0 approaches a frequency of the signal.

Finally, we perform a refinement of the approximated frequencies of the signal (32) by the method described in section 2.4. Computations are performed using an arithmetic of 32 decimal digits. To define the unfolded iterates $\{z_n^{(2^q,\omega_0,p)}\}$, we take $p = 2$ and $q = 6$. To refine the frequency, we select averaging order $p = 3$, and we compute up to $N = 2^{21}$ iterates of the unfolded signal $\{z_n^{(64,\omega_0,2)}\}$. Then, we extrapolate the frequency according to $\Theta^{(p,q)}$ in (27) by using all the possible values of q, i.e., for $3 \le q \le 21$. In the left plot of Figure 6 we show the real error in the extrapolation of the basic frequencies ω_1, ω_2, and ω_3, taking ω_0 as the exact value of the frequency to be computed. For $q = 21$ we get almost 20 correct digits. In the right plot of Figure 6 we repeat the computations for the frequency ω_1, now using different approximations ω_0 to unfold the curve. Specifically, we take $\omega_0 = \delta\omega_1$, with $\delta = 1$, 1.005, 1.01, and 1.015. We observe that the results do not depend essentially on the selected value of ω_0 and that the approximation $\frac{\omega_1}{2\pi} \simeq 0.415$, previously obtained looking at the peaks of $Z^{(64,2)}(\omega_0)$, belongs to the interval containing the selected values of ω_0, i.e., $\sqrt{2} - 1 \le \frac{\omega_0}{2\pi} \le 1.015 \times (\sqrt{2} - 1)$.

3. Study of a restricted three body problem. Let us consider two punctual masses (usually called primaries) which move in a circular orbit around their common center of mass according to the Kepler laws. The restricted three body problem (RTBP) describes the motion of a third particle (asteroid) on the vector field produced by these two primaries, assuming that the mass of the asteroid is so small that it does not affect the motion of the first two masses. As usual, we choose units of distance, time, and mass such that the gravitational constant is 1, the period of the primaries is 2π, and the sum of masses of the primaries is 1. With these units the distance between the primaries is also equal to 1. We denote by μ the mass of the smallest primary, $\mu \in (0, \frac{1}{2}]$. In what follows we take $\mu = 0.95388118036309677 \times 10^{-3}$, which corresponds to the Sun–Jupiter system, although the following presentation is common for any μ. For details, see [40].

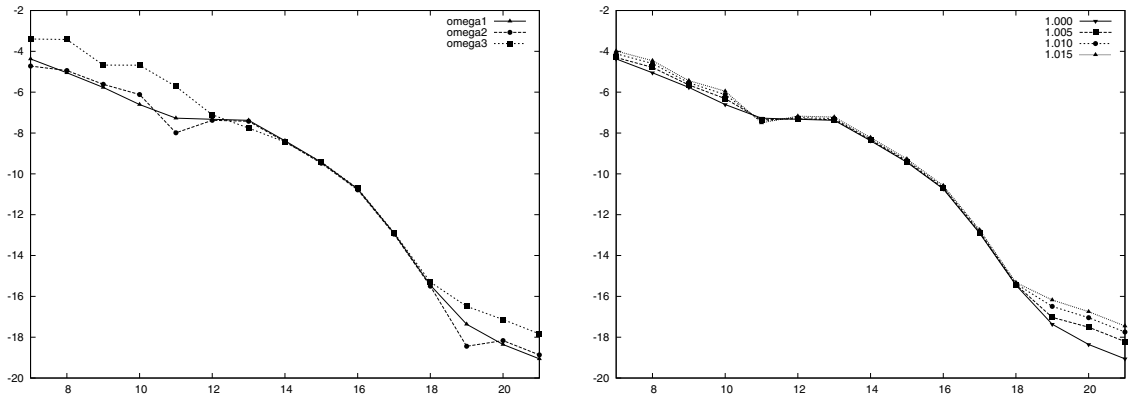

Figure 6. *Left: We plot the* $\log_{10}$ *of the error in the refinement of the frequencies* ω_1*,* ω_2*, and* ω_3 *of* (32) *(vertical axis) versus* q *(horizontal axis), where* 2^q *is the number of used iterates. See the text for details. Right: The same refinement process, now only for the frequency* ω_1*, by using different approximations* $\omega_0 \simeq \omega_1$ *to unfold the signal. We take* $\omega_0 = \delta\omega_1$*, with* $\delta = 1, 1.005, 1.01,$ *and* 1.015*.*

It is also usual to use a rotating (also called synodic) coordinate system with origin at the center of mass of the primaries, so that the two primaries are kept fixed on the x-axis. The x-axis points to the biggest primary, the z-axis points to the direction of angular motion of the primaries with respect to the center of mass, and the y-axis is defined such that we obtain an orthogonal, positive-oriented, system of reference. In this system, the primary of mass μ is at the point $(\mu - 1, 0, 0)$, and that of mass $1 - \mu$ is at $(\mu, 0, 0)$. Defining momenta $p_x = \dot{x} - y$, $p_y = \dot{y} + x$, and $p_z = z$, the equations of motion can be written in Hamiltonian form, with Hamilton function

$$H_0(x, y, z, p_x, p_y, p_z) = \frac{p_x^2 + p_y^2 + p_z^2}{2} + yp_x - xp_y - \frac{1-\mu}{r_S} - \frac{\mu}{r_J}, \tag{33}$$

where

$$r_S^2 = (x - \mu)^2 + y^2 + z^2, \qquad r_J^2 = (x - \mu + 1)^2 + y^2 + z^2.$$

This system has five equilibrium points belonging to the xy plane. Three of them (the Eulerian points L_1, L_2, and L_3) are on the x-axis, and the other two (the Lagrangian points L_4 and L_5) form an equilateral triangle with the primaries. The equilibrium point L_5 is

$$x = \mu - \frac{1}{2}, \quad y = \frac{\sqrt{3}}{2}, \quad z = 0, \quad p_x = -\frac{\sqrt{3}}{2}, \quad p_y = -\frac{1}{2} + \mu, \quad z = 0.$$

As the mass parameter of the Sun–Jupiter system is less than the Routh critical value $\mu_R \simeq 0.03852$, the point L_5 is linearly stable, with frequencies

$$\omega_1 = \left[\frac{1}{2}(1 - (1 - 27\mu(1-\mu))^{1/2})\right]^{1/2}, \quad \omega_2 = \left[\frac{1}{2}(1 + (1 - 27\mu(1-\mu))^{1/2})\right]^{1/2}, \tag{34}$$

and $\omega_3 = 1$ (this corresponds to the vertical oscillations). KAM theory can be applied in a straightforward way (see [9, 22]), thus obtaining plenty of invariant tori close to L_5. The

validity of the classical KAM approach applies only in a small neighborhood of the point, while the stability domain around L_5 is known to be much larger (pioneering results were presented in [34] for the Earth–Moon system). We refer the reader to the example of the region of Trojan asteroids (see the studies in [5, 11, 12, 13, 35]). The point L_4 is equivalent.

Our aim is to apply the methodology developed in section 2 to compute frequencies in the stability domain of L_5. We first consider in section 3.1 the planar RTBP, where the motion of the asteroid is restricted to the plane of the primaries, i.e., $z = 0$ and $p_z = 0$. In section 3.2 we deal with the full spatial problem given by (33). Finally, in section 3.3, we consider the so-called multicircular problem. This system is defined by adding to the RTBP the perturbation of planets moving in circular orbits around the center of mass of the Sun and Jupiter. The Hamiltonian for this perturbed problem, considering d additional planets of masses m_i, orbital radii a_i, and rotation frequencies $\hat{\omega}_i$, with $i = 1, \dots, d$, is given by

$$H_{MC}(x, y, z, p_x, p_y, p_z, t) = H_0(x, y, z, p_x, p_y, p_z) - m_i \sum_{i=1}^{d} \left(\frac{1}{r_i} + \frac{x \cos\theta_i}{a_i^2} - \frac{y \sin\theta_i}{a_i^2} \right), \tag{35}$$

where $\theta_i = \hat{\omega}_i t + \theta_i^{(0)}$ and

$$r_i^2 = (x - a_i \cos\theta_i)^2 + (y + a_i \sin\theta_i)^2 + z^2.$$

As considered in [20], in the computations presented we take into account the gravitational effect of Saturn, Uranus, Neptune, and Earth.

To numerically integrate the vector fields, we use a high-order Taylor method (the order depending on the desired precision). This method is an efficient way to perform both long term and highly accurate computations (to the extent that the use of explicit methods is a suitable choice). Although we coded our own integrator for the problem, very efficient packages have been developed for this purpose and are available to the public (see [2, 24]).

Remark 3.1. Using the Taylor method, we can integrate the vector field with a large time step—limited by the radius of convergence of the Taylor expansion of the solution. It can happen that the sampling time T used to built a quasi-periodic signal (see section 2.1) is smaller than the estimated radius of convergence of the series. In this case, we can save significant computational time by evaluating the computed Taylor polynomial (also called the jet) of the solution as long as we are inside the domain of convergence. Only when this evaluation is not possible must we recompute the Taylor expansion. For example, in the planar RTBP, a typical value for the radius of convergence is $h \simeq 1.4$, which is significantly larger than reasonable sampling times (we recall that $h = 2\pi$ corresponds to a rotation of Jupiter).

3.1. Planar case. Next we test the methodology of section 2 by performing the frequency analysis of initial conditions on the region of stability of L_5. This problem has already been studied in [13] using collocation methods, so it represents a nice test of the approach presented in this paper. Note that the planar problem has two degrees of freedom, and so, under isoenergetic nondegeneracy KAM conditions, invariant tori play the role of barriers in phase-space. This allows us to prove the nonlinear stability of L_5 in the planar RTBP for any $0 < \mu < \mu_R$, except for two values for which the point is unstable (see [32]). This leads to a

region of perpetual stability of L_5 in the planar case, even though in the spatial case we can only talk about "effective stability" (i.e., stability for a very long time).

Due to the characteristic "banana shape" of the stability region, it is very useful to introduce the adapted coordinates (see [12])

$$\begin{pmatrix} x \\ y \end{pmatrix} = \begin{pmatrix} \mu \\ 0 \end{pmatrix} + (1+\rho) \begin{pmatrix} \cos(2\pi\alpha) \\ \sin(2\pi\alpha) \end{pmatrix} \tag{36}$$

to parameterize initial conditions, so that L_5 corresponds to $\alpha = 1/3$ and $\rho = 0$. An initial condition of the form

$$x_0 = x(\alpha,\rho), \quad y_0 = y(\alpha,\rho), \quad p_{x_0} = -y_0, \quad p_{y_0} = x_0 \tag{37}$$

is considered to be in the domain of stability of L_5 if it librates around the equilibrium point. This means that the trajectory neither approaches the primaries nor encircles the main one. A criterion to detect whether a given trajectory escapes from L_5 is whether it eventually satisfies $y < -0.5$ (see [13]). Note that the initial conditions of the form (37) have zero synodic velocity and do not belong to any particular energy manifold of H_0 (i.e., do not have the same Jacobi constant).

From the results reported in [12, 13], we know that the initial conditions in (37) belonging to the stability domain of L_5 are contained in the box $(\alpha,\rho) \in [0.03, 0.42] \times [-0.015, 0.015]$ and that this domain is symmetric with respect to $\rho = 0$. To perform a systematic computation of the basic frequencies of this problem, we take a grid 500×250 of values of (α,ρ) in this box and consider the corresponding initial conditions (37). For any initial condition, we introduce the complex signal $z_n = x(n) + \mathrm{i}y(n)$, defined by evaluating the trajectory of (33) at time $t = n \in \mathbb{N}$. Since we take the sampling time $T = 1$, we expect the computed frequencies for the discretized signal to give frequencies of the signal of continuous variable defined by the trajectory—assuming that we have a good enough approximation of them. The numerical integration is performed using a Taylor method of order 24, working with double precision arithmetic and asking for local error 10^{-16}.

We are mainly interested in trajectories that belong to invariant tori with basic frequencies that are continuations of those of the elliptic point L_5. In analogy to a Lyapunov family of periodic orbits of an elliptic fixed point, we can refer to such tori as the (Cantor) family of Lagrangian invariant tori that emanates from L_5 (or simply to the family of invariant tori of L_5). We know that the set of initial conditions that belongs to a torus of this family has large relative Lebesgue measure if we are close enough to L_5 (see [9, 22]). Of course, it is clear that not any quasi-periodic solution in the region of stability of L_5 belongs to a torus of this family. For example, there are also "secondary invariant tori" created by the resonances, whose basic frequencies are not direct continuations of those of L_5; incidentally, secondary tori also have "different topology" as they do not turn around the point. Secondary tori are outside the scope of this systematic study.[5] There are other trajectories in the stability region

[5]To carry out the frequency analysis for a secondary torus we must perform a preliminary study of the signal in order to find a good set of approximate frequencies (see section 2.6). We also have to be aware that (at least) one of the frequencies is small and with small amplitude.

of L_5 that are not quasi-periodic but, for example, have stochastic behavior between the two-dimensional tori confining them. As the initial approximations to the frequencies will be taken close to those of L_5, we expect the approach of this paper to fail for any trajectory not in the family that emanates from L_5 (even if it survives the long time integration). Throughout the discussion we will abuse the notation introduced in (34), and we will refer to ω_1 and ω_2 as the frequencies of the family of invariant tori that emanates from L_5.

Initial approximations to the frequencies are obtained by taking advantage of the fact that frequencies move slowly with the initial conditions, so they remain very close to the planar frequencies (34) of the elliptic point (this is common to many problems in celestial mechanics). Specifically, we look for candidates in intervals of length 0.05 centered at the frequencies of L_5 (this length is suggested by the results reported in [12, 13]). We evaluate the first $L = 1024$ iterates, and, following section 2.6, we compute $Z^{(1024,2)}(\omega_0)$ for 60 values of ω_0 in each of the two intervals, thus obtaining suitable candidates for the frequencies ω_1 and ω_2. This criteria has both a negligible computational cost and a good global performance for the range of orbits considered. We also use these iterates to compute a rough approximation $\Gamma^{(0,2,10)}$ of the average of z_n, using the method in section 2.5. We redefine the signal by subtracting this estimated average, i.e., $z_n \mapsto z_n - \Gamma^{(0,2,10)}$. In this way we improve the performance of the unfolding procedure (see Remark 2.20).

Given an approximation of a frequency, we unfold the signal by applying the methodology of section 2.3 with $p = 2$ (second order unfolding) and $q = 10$ (i.e., we use $L = 1024$ iterates to define any unfolded iterate). We refine the frequencies by the averaging-extrapolation method of section 2.4, taking $p = 4$ and computing $2^{16} = 65536$ iterates of the signal at most. We stop the computations if two consecutive approximations to the frequencies differ by less than 10^{-12}. If this tolerance is not reached along the integration, then we store the last values for the frequencies that we have computed as well as the estimated error. The maximum time that we integrate a trajectory is $t_{\max} = 2^{10} + 2^{16} = 66560$ (i.e., about 10593 revolutions of Jupiter). If during the integration we detect that the trajectory escapes (i.e., it satisfies $y < -0.5$), then the corresponding initial condition is rejected, and we do not associate any frequency to it.

In the left plot of Figure 7 we show the points that have not been rejected. Of course, trajectories for these initial conditions can escape if $t_{\max}$ is increased. Due to the fact that KAM tori are sticky (see [33]), a huge value of $t_{\max}$ is required to obtain a sharp estimation of the boundary of the domain of stability. For example, in the computations presented in [13], trajectories are integrated up to 200 Myears in physical time (about 16777216 revolutions of Jupiter). Characterizing this frontier of stability is not among the aims of our approach. Nevertheless, it is worth paying attention to the behavior of the method in this zone. Hence, we plot in black those points where the refinement of the frequency has a "bad performance" (when the sum of the final estimated errors for ω_1 and ω_2 is larger than $6 \cdot 10^{-6}$) and in red the remaining ones. If we compare with the domain of stability reported in [13, Figure 10], it seems that the black points are going to escape eventually (note that they accumulate at the boundary). Hence, the information given by the convergence of the method can allow us to detect some escaping trajectories before they leave the domain of influence of L_5, thus obtaining an approximation of the frontier of stability using a short range integration. We come back to this point later.

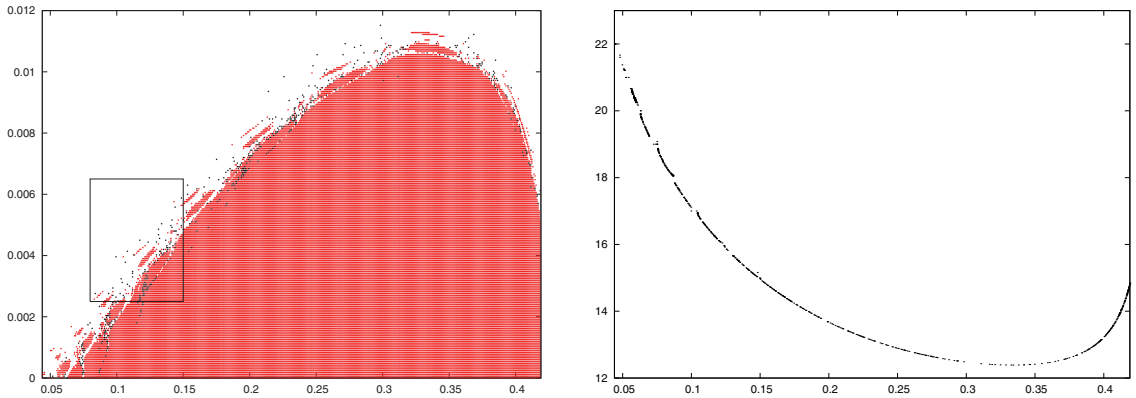

Figure 7. *Left: We plot ρ (vertical axis) versus α (horizontal axis) for the initial conditions (37) according to the following criteria: White for those points that escape before $t_{\max} = 66560$, black if the estimated error for the computed frequencies is larger than $6 \cdot 10^{-6}$, and red otherwise. Points within the marked rectangle will be considered again in Figure 12. Right: We show the graph $\omega_1/2\pi$ versus α when $\rho = 0$ only for those points with a final error for the frequencies smaller than 10^{-6}.*

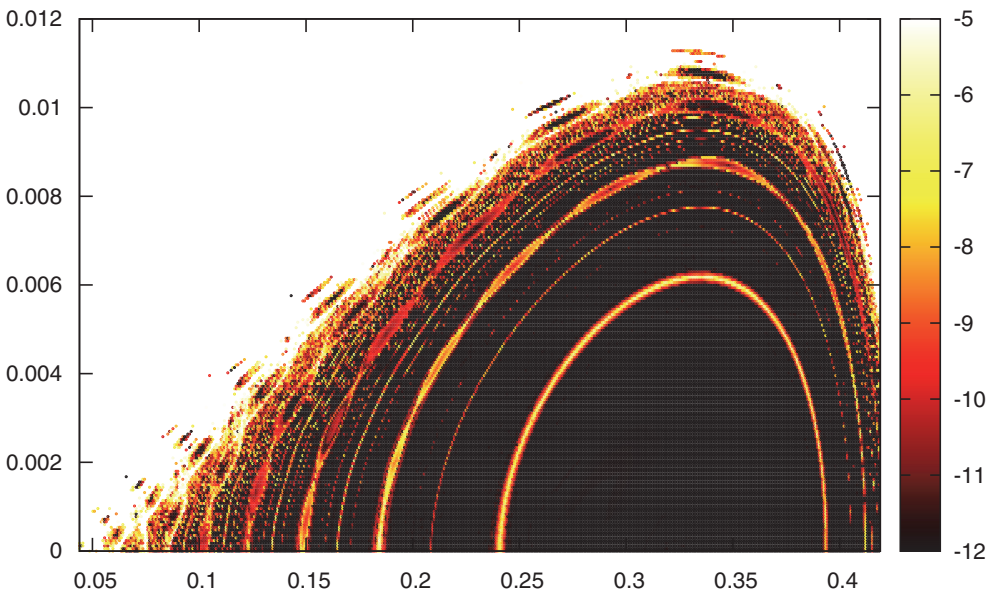

Figure 8. *We plot ρ (vertical axis) versus α (horizontal axis) labeling the initial conditions (37) for the planar RTBP. We represent the error in the computation of the frequencies using a $\log_{10}$ color scale.*

In Figure 8 we plot the initial conditions (37) according to the convergence of the method. The palette of colors represents the sum of the final errors (in $\log_{10}$ scale) in the computation of ω_1 and ω_2. We select a color palette from white (error 10^{-5}) to black (error 10^{-12}). This palette is also used in subsequent figures. For a "good initial condition" (i.e., belonging to a three-dimensional invariant torus with frequencies close to those of L_5 and far from resonance),

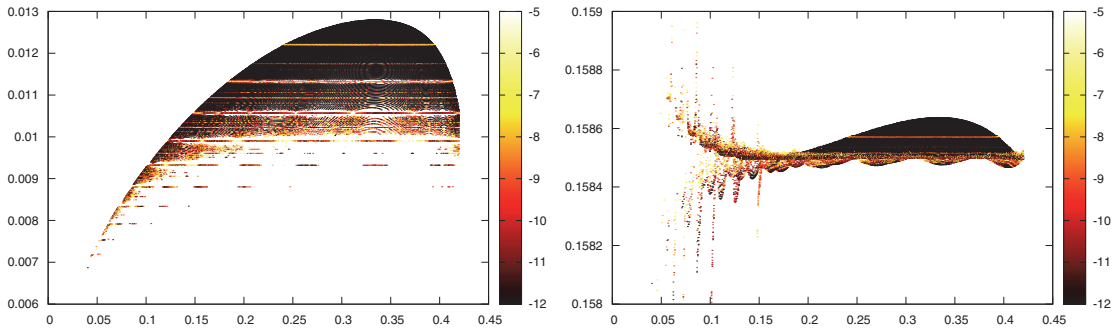

Figure 9. *For the planar problem, we show $\omega_1/2\pi$ (left plot) and $\omega_2/2\pi$ (right plot) versus α for every ρ. We plot only those points with total error smaller than 10^{-5}.*

we require about 3000 Jupiter revolutions to reach the requested tolerance of 12 digits. In Figure 9 we show the computed frequencies $\omega_1/2\pi$ (left plot) and $\omega_2/2\pi$ (right plot), and the quotient ω_2/ω_1 is shown in Figure 10. As previously mentioned, the frequencies present a small range of variation. We recall that we are asking the frequencies to be Diophantine (with a constant C in (2) not too small) in order to justify the validity of our averaging-extrapolation approach, so it is not surprising that the convergence of the method has problems as we approach a resonant zone. The final estimated error manifests this fact. Resonances correspond to $\omega_2/\omega_1 \in \mathbb{Q}$, and this color palette turns out to be very useful in visualizing them (the integer resonances and the semi-integer resonances as well) in Figure 10. Another way to visualize these resonances is to fix a value of ρ and to plot the graph $\alpha \mapsto \omega_2/\omega_1$. This is done in the right plot of Figure 7 for $\rho = 0$. The result resembles a Devil's Staircase, which is a classical way to refer to the graph of the rotation number of a family of circle maps as a function of a parameter. Recall that a Devil's Staircase for a family of circle maps is a continuous graph, but here we observe holes for the parameters for which there are no tori.

As discussed in section 2.5 (see Remark 2.19), computing the amplitude corresponding to a given frequency is a very simple and reliable test to verify the computations. Although we rely on the fact that the refined frequencies remain close to the first approximation to validate the computations presented above, in the following we illustrate this test with a particular case. We consider the trajectory corresponding to $\alpha = 0.2211$ and $\rho = 0$ that has frequency

$$\omega_1/2\pi \simeq 0.011933549909.$$

We implement Proposition 2.18 to compute the amplitude corresponding to ω_1, taking $k^* = e_1 = (1, 0)$ and $p = 4$. Using $q = 15$, we obtain the approximation (clearly different from zero)

$$\hat{\gamma}_{e_1} \simeq \Gamma^{(e_1,4,15)} = 0.241593382 + 0.07606123\,\mathrm{i},$$

with an estimated error $3 \cdot 10^{-9}$.

Let us summarize some statistics of the obtained results. After integrating up to $t_{\max}$, we have that 54.8% of initial conditions escape from the region of libration around L_5. For 75.3% of the remaining trajectories, the total estimated error for the frequencies is smaller than 10^{-11}. We may consider that they belong to quasi-periodic invariant tori with (good)

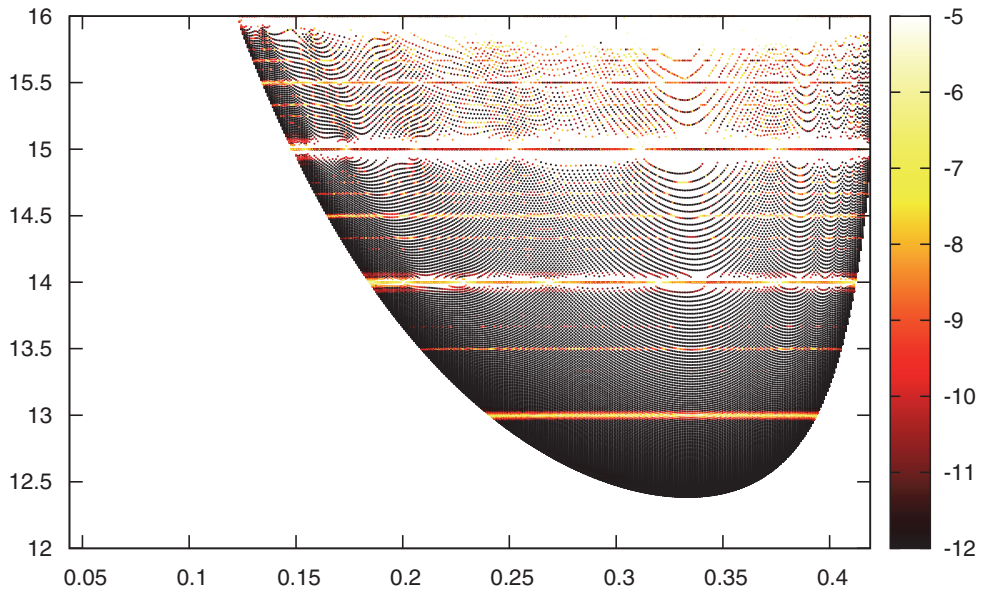

Figure 10. *Computation of frequencies in the planar problem. We show ω_2/ω_1 versus α for every value of ρ. We restrict the figure to $\omega_2/\omega_1 \in [12, 16]$.*

Diophantine frequencies. Only for 1.04% of the trajectories that do not escape the frequencies have been approximated with an error larger than $5 \cdot 10^{-6}$. Many of these trajectories are close to the boundary of the region of stability and some of them will escape eventually after a larger integration. These numbers do not match exactly with the behavior of the method reported in [13] since here we deal only with Lagrangian invariant tori of frequencies close to those of L_5. In [13] secondary tori are also taken into account.

Another phenomenon that we want to illustrate is the effect of the sampling time T (see section 2.1) in the computation of the frequencies. To this end, we consider a particular trajectory, given by $\alpha = 0.2952$ and $\rho = 0$, that has frequencies

$$\omega_1/2\pi \simeq 0.012689145311, \qquad \omega_2/2\pi \simeq 0.158623295518. \tag{38}$$

From this trajectory, we introduce quasi-periodic signals of the form $z_n = x(nT) + \mathrm{i}y(nT)$, $n \in \mathbb{N}$, for different sampling times $T \in (0, 4)$. Recall that, after computing a frequency $\bar{\omega}$ in terms of the sampling time T, we expect $\bar{\omega}/T$ to be a frequency of the original trajectory (at least for T not too large). We try to approximate ω_1 for different values of T according to the same implementation details used before. A first approximation of the frequency is obtained from the study of $Z^{(2^{10},2)}(\omega_0)$. Then, to unfold the signal we use $p = 2$ and $L = 2^{10}$, and to compute the frequencies we use $p = 4$ and up to $N = 2^{14} = 16384$ iterates. The estimated error in the computation of ω_1 as a function of T is shown in the left plot of Figure 11. We observe that for small values of T the performance of the method improves when T increases. Beyond resonances, this phenomenon is clear since the total integration time is proportional to T. This improvement stops when 14 correct digits have been obtained (we recall that

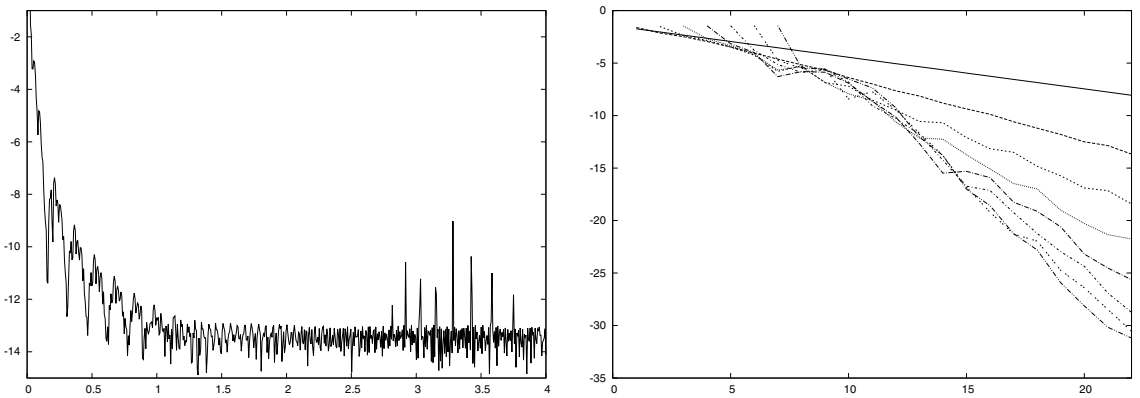

Figure 11. *Left: Error (in* $\log_{10}$ *scale) versus the sampling time* T *in the computation of* ω_1 *in the planar problem for* $\alpha = 0.2952$ *and* $\rho = 0$ *(see (37)). Right: Error (in* $\log_{10}$ *scale) versus* $q = \log_2 N$ *in the computation of* ω_1 *for* $\alpha = 0.2211$ *and* $\rho = 0$ *for different extrapolation orders* $p = 0, \ldots, 7$ *(we join consecutive points by lines).*

computations are performed using double precision arithmetic). For largest values of T, the method loses efficiency when T is close to a resonant value of the form $T \approx 2\pi m/\langle \omega, k\rangle$, for some $k \in \mathbb{Z}^2$ and $m \in \mathbb{N}$. Some of the main resonances observed in the plot correspond to $m = 1$ and $k = (2, 2)$, $(1, 2)$, $(0, 2)$, $(-1, 2)$, and $(-2, 2)$. The values of T for these resonances are $T \simeq 2.918644$, 3.030893, 3.152122, 3.283453, and 3.426203.

Remark 3.2. Since ω_1 is small, we only lose information on the frequency of the trajectory due to accumulated turns of the discretized signal if we take $T > 2\pi/\omega_1 \simeq 78.8$. In general, if we want to get rid of the effect of the accumulated turns due to the selection of T, we can proceed as follows. Let us compute two numerical values $\omega^{(j)}$ for a frequency of the discretized signal—associated to the same approximate frequency of the trajectory—after considering two "unrelated" values of the sampling time, $T = T_j$, $j = 1, 2$. If we set $\widetilde{\omega}^{(j)} = \omega^{(j)}/T_j$, then a true value for the frequency of the trajectory can be identified by inspection of the coincidences between the sets $\{\omega^{(j)} + 2\pi m/T_j \,:\, m \in \mathbb{Z}^r\}$ for $j = 1, 2$.

Following section 2.4, we can compute frequencies with high accuracy due to the asymptotic behavior $\mathcal{O}(1/N^{p+1})$ of the error. However, since computations have been performed using double precision arithmetic, the maximum accuracy for the frequency is attained quickly, and the results cannot be improved by considering more iterates or higher extrapolation orders. We refer the reader to [29, 30, 36] for detailed discussions in terms of computations performed using 32 and 64 digit arithmetic. To illustrate the behavior of this methodology for large values of p and q, we present some computations performed using 32 digit arithmetic. We integrate the vector field using a Taylor method of order 36 and asking for a tolerance of 10^{-32}. As an example, we tackle the computation of ω_1 for the trajectory given by $\alpha = 0.2211$ and $\rho = 0$. As sampling time we take $T = 1$, and as initial approximation of the frequency we take $\omega_1/2\pi \simeq 0.01193354991$ (the value we have previously obtained using double precision arithmetic). As noted before, once the signal has been "successfully unfolded," the potential accuracy that we can reach for the frequency is not conditioned by the distance to a rigid rotation of the projected signal. In other words, improving the computation of the frequency

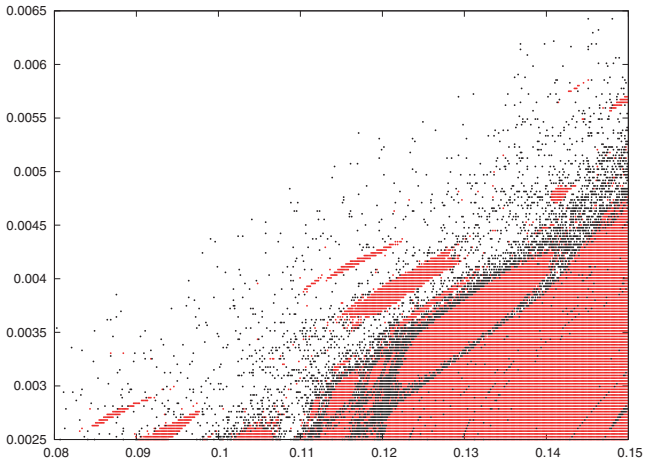

Figure 12. *We plot ρ versus α for the points inside the marked rectangle of Figure 7. We use white for those conditions that escape before $t_{\max} = 8192$, black for those points where the final estimated error in the computation of the average is larger than 10^{-4} after $t_{\max}$, and red otherwise.*

by the averaging-extrapolation method of section 2.4 does not require increasing the values $p = 2$ and $L = 2^{10}$ used to unfold the signal. Results are shown in the right plot of Figure 11. The vertical axis is the $\log_{10}$ of the error of the method, which gives (minus) the number of correct decimal digits (the error is estimated by comparing two consecutive computations). The horizontal axis means $q = \log_2 N$, where $N = 2^q$ is the number of iterates used to compute the frequency. The error-curves correspond to different values $p = 0, \dots, 7$ of the extrapolation order (recall that if $p = 0$, then the method reduces to applying the definition of rotation number). For $N = 2^{22}$ the curves are ordered from top to bottom by increasing value of the extrapolation order p. One can check that, for a sufficiently large value of q, the slope of the curves tends to be $-(p+1)\log_{10} 2$, as expected, due to the asymptotic behavior of the error.

As observed in Remark 2.20, the computation of the average of the discretized signal is a simple (and fast) indicator of candidates for quasi-periodic solutions (without computing any frequency). To show the features of this approach, we take a 500×250 grid of initial values of $(\alpha, \rho) \in [0.08, 0.15] \times [0.0025, 0.0065]$. This corresponds to a zoom of the left plot of Figure 7 and of Figure 8 that contains part of the boundary of the domain of stability (see the marked rectangle in Figure 7). Then, we use the algorithm described in Proposition 2.18 to compute the average of the corresponding trajectories. Specifically, we take $p = 4$ and at most $2^{13} = 8192$ iterates in formula (29), with sampling time $T = 1$. As we only want to detect such trajectories for which the average seems to converge, but not an accurate value for it, we stop the computations if the difference between two consecutive iterations, i.e., $|\Gamma^{(0,4,q)} - \Gamma^{(0,4,q-1)}|$, is less than 10^{-8}. In Figure 12 we show the points that have not been rejected after $t_{\max} = 8192$. We plot in black those points where the computation of the average has a bad performance (the final estimated error is larger than 10^{-4}) and in red the remaining points.

Notice that looking at the red points we obtain a nice approximation of the boundary of stability using a relatively short integration time—only about 1304 Jupiter revolutions at

most. Compare with the 16777216 revolutions (at most) used in [13] to accurately characterize the boundary in terms of the criterion that escaping solutions eventually reach $y < -0.5$. In other words, we note that many points which will eventually escape after a long integration are still librating around L_5 after the considered integration time, but the accuracy of the average is less than 10^{-4}. We emphasize that the computation of the average is useful for detecting initial conditions on secondary tori. However, it has the inconvenience that some of these "bad" points correspond to trajectories that are confined inside the domain of stability but that do not belong to any invariant torus of the system.

Although analyzing the behavior of the computation of the average by averaging and extrapolation is not the purpose of this work, we think that this approach is interesting for purposes of studying a wide set of problems in a systematic way—to detect either escaping or chaotic trajectories—since the average can be computed with high accuracy at a very low computational cost. Moreover, this has the advantage of being a general criterion, independent of the problem at hand (we do not require particular characterizations of escaping orbits such as the criterion $y < -0.5$).

3.2. Spatial case. Now we consider the full Hamiltonian (33). In the spatial RTBP we cannot properly speak about the stability domain of L_5, as the three-dimensional KAM tori of the system do not act as barriers for the solutions in the five-dimensional energy manifolds. Hence, beyond the set of positive Lebesgue measure defined by these invariant tori, for a general trajectory of the spatial RTBP we can only ask for effective stability (i.e., stability for long times in the aim of the classical Nekhoroshev estimates).

It is known that the extension to $z > 0$ of the domain of stability of L_5 has a paraboloid shape. Then, a good parameterization for the initial conditions is (we refer the reader to [39])

$$\begin{pmatrix} x \\ y \\ z \end{pmatrix} = \begin{pmatrix} \mu \\ 0 \\ z \end{pmatrix} + (1 + \rho - \sqrt{\psi(z^2)}) \begin{pmatrix} \cos(2\pi\alpha) \\ \sin(2\pi\alpha) \\ 0 \end{pmatrix}, \tag{39}$$

where

$$\psi(w) = 1 - \frac{1}{2}w + \frac{3}{2^5}w^2 - \frac{1}{2^8}w^3 - \frac{25}{2^{13}}w^4 + \frac{33}{2^{16}}w^5 + \frac{175}{2^{20}}w^6 - \frac{497}{2^{23}}w^7 - \frac{4401}{2^{29}}w^8 + \cdots .$$

We fix $\rho = 0$, we take a 500×500 grid of values of $(\alpha, z) \in [0.03, 0.42] \times [0, 1]$, and we consider initial conditions with zero synodic velocity parameterized as

$$x_0 = x(\alpha, 0, z), \quad y_0 = y(\alpha, 0, z), \quad z_0 = z, \quad p_{x_0} = -y_0, \quad p_{y_0} = x_0, \quad p_{z_0} = 0. \tag{40}$$

For any of these trajectories we introduce the complex signal $z_n = x(n) + \mathrm{i}y(n)$ by taking again sampling time $T = 1$.

We compute the frequencies ω_1, ω_2, and ω_3 of the invariant tori emanating from the point L_5. Implementation parameters are very similar to those used in the planar case (see section 3.1). The numerical integration is performed by using a Taylor method of order 24, working with double precision arithmetic, and asking for local error 10^{-16}. Initial approximations to the basic frequencies are obtained starting from the information of the planar

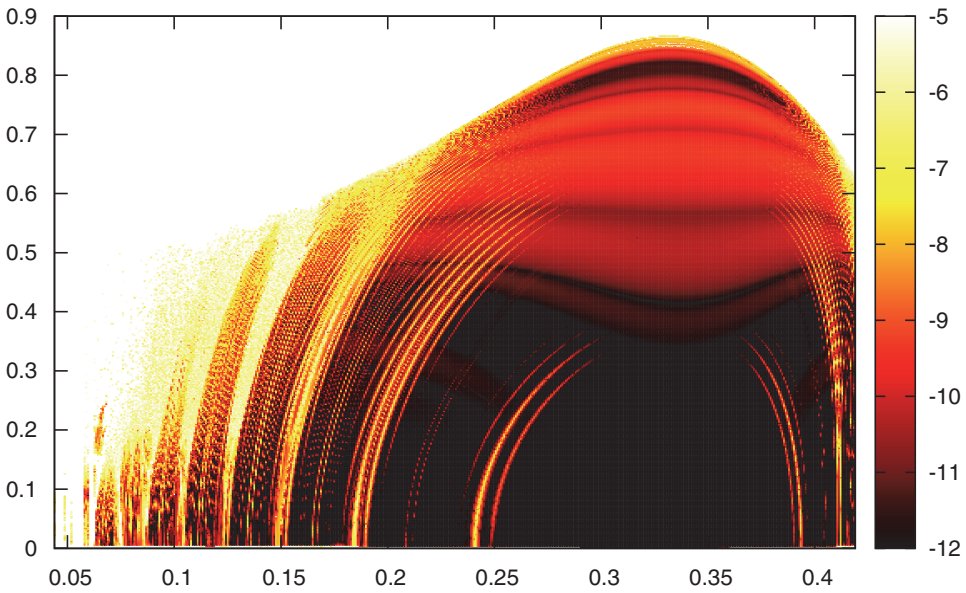

Figure 13. *We plot z (vertical axis) versus α (horizontal axis) labeling the initial conditions in the spatial problem according to (40). We represent the error in the computation of the three basic frequencies using a $\log_{10}$ color scale.*

problem. Hence, for $z \simeq 0$, to approximate ω_1 and ω_2 we look for peaks close to the frequencies computed for the planar case, and to approximate ω_3 we look for a peak close to 1. After this triplet of frequencies has been refined, we increase the value of z, and we use the previously obtained frequencies as reference values to look for candidates (peaks) for the new ones. We look for peaks in intervals of length 0.0032 around each of these reference values by computing $Z^{(1024,2)}(\omega_0)$ (see section 2.6) for 60 values of ω_0 in any of the three intervals. It is worth mentioning that ω_2 is so close to ω_3 that we have to pay attention to this fact to guarantee that we have a good approximation of any of them. Otherwise, combination of unfolding and refinement converges to the same result for the two approximations.

As in the planar case, we use the method in section 2.5 to compute a rough approximation of the average of the signal, and we redefine z_n by subtracting this average. Specifically, we introduce $z_n \mapsto z_n - \Gamma^{(0,2,10)}$. Then, we unfold the signal by applying the methodology of section 2.3 with $p = 2$ (second order unfolding) and $q = 10$ (i.e., we use $L = 1024$ iterates to define any unfolded iterate). We refine the frequencies by the averaging-extrapolation method of section 2.4, taking $p = 4$ and computing $2^{16} = 65536$ iterates of the signal at most. We stop the computations if two consecutive approximations to the frequencies differ by less than 10^{-12}.

In Figure 13 we plot the considered initial conditions (40) colored according to the convergence of the method. The palette of colors represents the sum of the estimated errors (in $\log_{10}$ scale) in the approximation of the three frequencies. Let us observe that set of points where the computation of the frequencies is not performed accurately corresponds to the "geo-

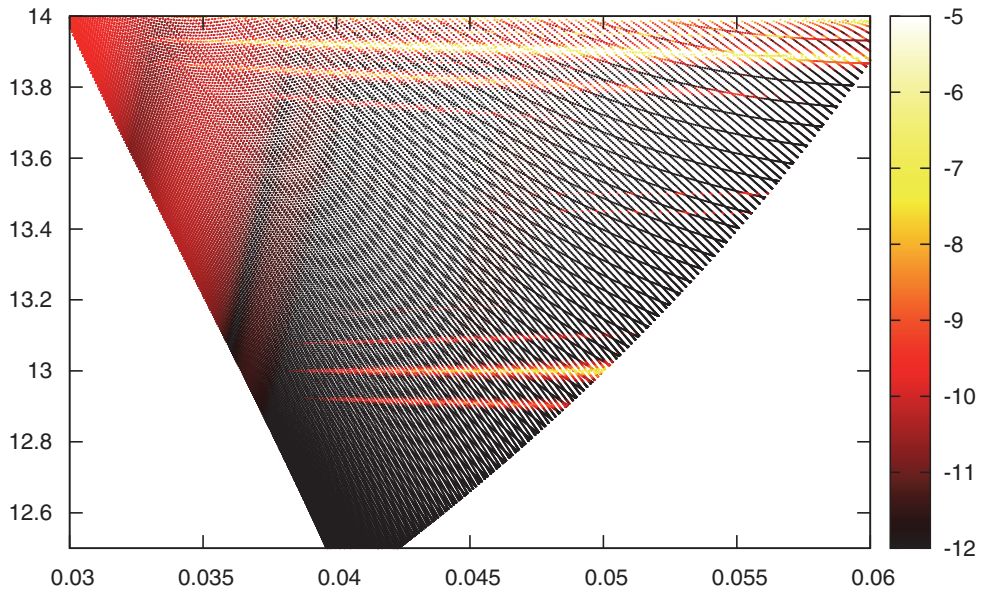

Figure 14. *Left: We plot the quotients ω_2/ω_1 (vertical axis) versus $(\omega_3-\omega_2)/\omega_1$ (horizontal axis) for a zoom of the selected grid of conditions in the spatial problem according to (40). We use the same color palette for the error as in Figure 13.*

metrical continuation" to $z>0$ of the resonances observed in Figure 8 for $\rho=0$. We have repeated the computations for initial conditions defined as in (40), but for different values of ρ in (39), obtaining analogous results.

In Figure 14 we represent some combinations of the frequencies associated to the points in Figure 13. We plot a zoom to enhance the structure of the plot. We use the same $\log_{10}$ color palette for the error as in Figure 13 in order to visualize the main resonances. Note that resonances correspond to vanishing integer combinations of the three frequencies. As ω_2 and ω_3 are very close, we show ω_2/ω_1 versus $(\omega_3-\omega_2)/\omega_1$. Apart from the resonances, we observe that in the plot the points look as if they were distributed in curves. A natural explanation is that the map

$$(\alpha,z)\longmapsto\left(\frac{\omega_3-\omega_2}{\omega_1},\frac{\omega_2}{\omega_1}\right)$$

behaves as a diffeomorphism on a Cantor-like set of large Lebesgue measure. Since we plot the points corresponding to the grid of values of (α,z) by moving through coordinate lines, we observe the image of these lines as smooth curves.

Finally, we present some statistics of the obtained results. We obtain that 61.18% of the trajectories do not escape after integrating up to $t_{\max}$. For 2.17% of these trajectories, the sum of the (estimated) errors in the computation of the three frequencies is larger than $5\cdot10^{-6}$. We expect most of them to escape after a longer (possibly large) integration. For 45.45% of them, the sum of the errors is smaller than 10^{-11}. We hope that these trajectories belong to quasi-periodic invariant tori whose basic frequencies are "very" Diophantine and close to the

Table 1
Frequencies, masses, and radii of the planets used in (35).

Planet	$\hat{\omega}_i$	m_i	a_i
Neptune	0.92801432138537394	5.1464752074960787e-5	5.7788760748791814
Saturn	0.59716051258412511	2.8561327940941584e-4	1.8335242195766197
Uranus	0.85880670883551138	4.3620791653297386e-5	3.6880511883932363
Earth	-0.1862408594090464	3.0375324347911519e-6	0.1923832582416737

normal ones of L_5.

3.3. Multicircular problem. Now we consider the Hamiltonian (35), where the effect of additional planets is taken into account (see Table 1). Specifically, we consider the effect of Saturn, Uranus, Neptune, and Earth, the first perturbation being the most significant. This model was studied in [20], where the four-dimensional invariant torus that replaces the point L_5 was computed. Note that we expect the invariant tori of the autonomous spatial system to enlarge their dimension by adding the frequencies of the planets (see [23, 38]). Indeed, the natural quasi-periodic solutions of (35) have seven basic frequencies, even though four of them are known a priori. We use the methodology introduced in this paper to analyze the abundance of quasi-periodic solutions around the point L_5 (indeed, around the four-dimensional torus that replaces it) by computing the remaining three basic frequencies (as a continuation of the normal ones of L_5) for the stable solutions. We keep the notation ω_1, ω_2, and ω_3 for the continuation of the frequencies of L_5, and we denote by $\hat{\omega}_1$, $\hat{\omega}_2$, $\hat{\omega}_3$, and $\hat{\omega}_4$ the frequencies of the forcing.

We take the same initial conditions (40) as in section 3.2, using the same grid of values of (α, z) to parameterize (39), and we define the complex signal $z_n = x(n) + \mathrm{i}y(n)$ by integrating (35). The implementation details are the same as those in section 3.2, including the strategy for computing initial approximations to the frequencies (performing continuation with respect to z). However, since the numerical integration of this problem is computationally more demanding than the spatial RTBP, we restrict the maximum number of iterates to $2^{14} = 16384$ (about 2607 Jupiter revolutions), and we stop the computations if two consecutive approximations to the frequencies differ by less than 10^{-8}. From the qualitative point of view, the obtained results look similar to those for larger integration times. Results are shown in Figure 15.

As done previously, we use a $\log_{10}$ color palette to represent initial conditions according to the performance of the method. Comparing with Figure 13, we observe that the quasi-periodic perturbation produces significant changes in the region of stability around the torus replacing L_5. Indeed, the size of the domain of effective stability remains essentially the same, but a larger quantity of invariant tori of the RTBP is destroyed by the perturbation, especially in the horizontal direction. In particular, we find quasi-periodic solutions in a region that is above (in the vertical direction) the torus that replaces L_5. This is consistent with the fact that this torus is linearly stable. Further, this is also in accordance with the study presented in [19] for the bicircular problem Earth–Moon–Sun, in which the periodic orbit replacing L_5 turns unstable, even though stable motion is still obtained in the vertical direction (of course the effect of Saturn in the Sun–Jupiter case is not as dramatic as the effect of Sun in the

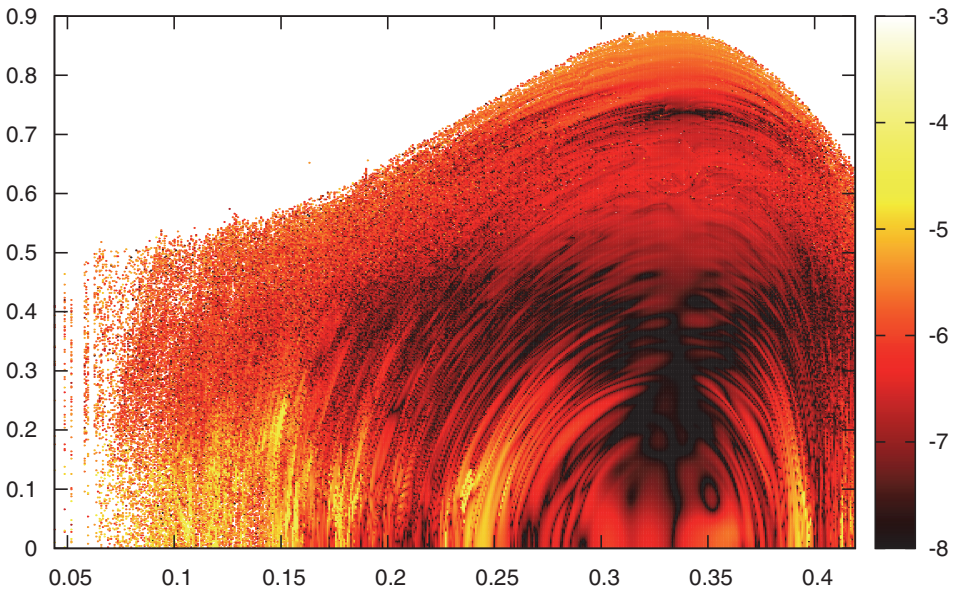

Figure 15. *We plot z (vertical axis) versus α (horizontal axis) labeling the initial conditions in the multicircular problem according to (40). We represent the error in the computation of the three basic frequencies using a $\log_{10}$ color scale.*

Earth–Moon case).

As far as statistics are concerned, we have that 59.57% of the trajectories have not escaped after integrating up to $t_{\max}$. This number is slightly smaller than that for the spatial RTBP (the "unperturbed problem"), but in this case $t_{\max}$ is significantly smaller. Comparing with the RTBP, we expect a larger number of trajectories to escape for large values of $t_{\max}$. In addition, only 4.56% of the points that have not escaped present an estimated error for the three frequencies smaller than 10^{-7}. Recall that we are integrating at most up to $t_{\max} = 16384$, and we can obtain higher precision for the frequencies by taking a larger integration time.

Next, we study the frequencies of a particular orbit using a larger number of iterates. We select an initial condition that is known to be on an invariant torus. Specifically, we consider the two-dimensional torus that replaces L_5 in presence of Saturn and Neptune. This torus, which has basic frequencies $\hat{\omega}_1$ and $\hat{\omega}_2$ (those of Saturn and Neptune), was numerically computed in [20, bottom plot of Figure 5], and it is characterized by the initial condition

$$x = -0.49507899400971284, \quad y = 0.86774513932356423, \quad z = \dot{x} = \dot{y} = \dot{z} = 0. \tag{41}$$

We consider first the computation of the average $\hat{\gamma}_0 \simeq \Gamma^{(0,p,q)}$ (see Proposition 2.18) of this quasi-periodic trajectory. The numerical integration is performed using a Taylor method of order 24 working with double precision arithmetic and asking for local error 10^{-16}. In Figure 16, we show the $\log_{10}$ of the estimated error $|\Gamma^{(0,p,q)} - \Gamma^{(0,p,q-1)}|$ versus $q = \log_2 N$ for different values of the averaging order p. As expected, the behavior is analogous to Figure 11. Note that if we take $p = 4$ and $q = 14$, we approximate the average almost with double precision.

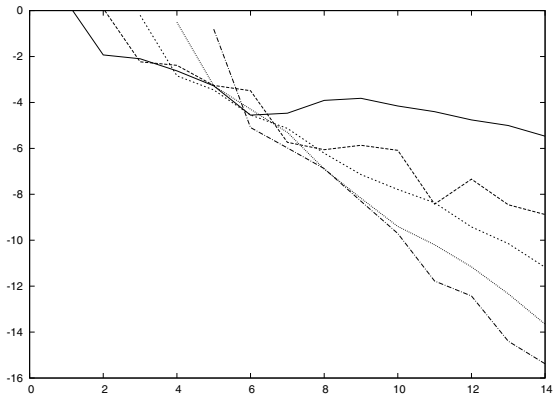

Figure 16. *Study of the torus that replaces the point L_5 in the presence of Saturn and Neptune. We plot the error corresponding to the computation of the average (in $\log_{10}$ scale) versus $q = \log_2 N$ for different values of p.*

Table 2

Computed frequencies of the torus that replaces the point L_5 in the presence of Saturn and Neptune for different values of $q = \log_2 N$.

q	$\hat{\omega}_1$	$\hat{\omega}_2$
5	0.92865398014370974316527666946892 9	0.59938232953729266065185106633565 8
6	0.92807469814140036788640536562180 2	0.59735379946313273186781352197071 9
7	0.92801140604021007300764932866282 3	0.59717068328729461333716691243888 0
8	0.92801298119005888297013206254000 1	0.59716086343389047804873404232335 3
9	0.92801478329309208766499461961498 8	0.59716052139442006132383078719337 8
10	0.92801466096225075039675662675976 0	0.59716051275981603532365420083179 2
11	0.92801428406498441748685765131248 9	0.59716051258785879360701974615371 0
12	0.92801432172469779232050417360576 5	0.59716051258417503382800105365971 6
13	0.92801432137662458255376836223646 8	0.59716051258412611211750050442798 7
14	0.92801432138574930396758981302560 8	0.59716051258412511919566751965533 59
15	0.92801432138537375478996454193218 6	0.59716051258412511022509855229960 0
16	0.92801432138537387242297014578941 9	0.59716051258412511000436887409902 9
17	0.92801432138537394144743730572816 2	0.59716051258412511000003565958452 8
18	0.92801432138537394000019401875018 6	0.59716051258412511000000085239470 2
19	0.92801432138537393999973972488688 0	0.59716051258412511000000001682108 3
20	0.92801432138537394000000491013765 2	0.59716051258412511000000000014270 0

Finally, we face the computation of the frequencies $\hat{\omega}_1$ and $\hat{\omega}_2$ from the discretized trajectory of (41) by unfolding, averaging, and extrapolation. These frequencies are known, but we want to show that their computation is carried out with high precision by our approach. Recall that these frequencies come from a "small" quasi-periodic perturbation, so the effectiveness of the unfolding process is not secured a priori. Computations are performed using an arithmetic of 32 decimal digits. The numerical integration is carried out using a Taylor method of order 36 and asking for a tolerance of 10^{-32}. Although we could use the values in Table 1 as "approximations" to the frequencies for the unfolding, we act as if they are unknown, and we look for candidates for the frequencies looking for peaks in the intervals $[0.88, 0.95] \ni \hat{\omega}_1$ and $[0.56, 0.64] \ni \hat{\omega}_2$. Specifically, we use the criteria described in section 2.6, computing

$Z^{(1024,2)}(\omega_0)$ for 60 values of ω_0 in each interval. As before, to improve the performance of the unfolding procedure, we redefine the signal by subtracting a (rough) approximation of its average, i.e., $z_n \mapsto z_n - \Gamma^{(0,2,10)}$ (see Remark 2.20). To unfold the signal we use $p = 2$ and $L = 1024$. To refine the frequencies of Saturn and Neptune, we use $p = 5$ and compute up to $N = 2^{20}$ iterates of the unfolded signal. In Table 2, we present the approximation of both frequencies for different values of $q = 5, \dots 20$, where 2^q is the number of iterates of the unfolded signal. Notice that the method performs very well in high precision, and we obtain the digit 0 beyond the truncated precision of the initial data.

4. Conclusions and final remarks. In this paper we have presented a methodology to perform frequency analysis of analytic quasi-periodic signals with Diophantine basic frequencies. Given a good approximation of any of the frequencies, we can refine it up to high precision at a moderate computational cost and at low memory requirements. The method is very flexible and self-contained in the sense that it also allows us to obtain initial approximations of the frequencies when we have no previous information on them. Such initial approximations are more accurate than those obtained by straight use of DFT.

A remarkable feature of our approach it that refining a particular frequency does not require any information on the other frequencies or simultaneously computing any Fourier coefficient of the signal. The accuracy of the method is not constrained by the number of significant Fourier harmonics required to approximate the quasi-periodic signal or by the dimension of the vector of basic frequencies of the problem. Fourier coefficients can be obtained a posteriori by slightly modifying the procedure for calculating the frequencies.

Among the strengths of our approach is the fact that it is dynamically coherent with the problem. Indeed, algorithms preserve the quasi-periodic structure of the original signal. No spurious frequencies are added due to the truncation of the signal to a finite sample, and it is not necessary to turn the signal into a periodic one in order to magnify its dominant frequencies.

The presented algorithms are extremely simple to code and optimize. The largest set of data required to store in memory is an array of length L that corresponds to the number of iterates used to define an iterate of the unfolded signal. The time cost of computing an unfolded iterate is essentially the cost of evaluating an iterate of the original signal and performing $4p_u$ products (see Appendix A, where p_u is the order of the unfolding). The cost of a frequency refinement of order p_r, using N iterates of the unfolded signal, is essentially the cost of evaluating N unfolded iterates and performing $2p_r$ products. There are several parameters to optimize for a given particular problem (sampling time, averaging orders, etc.). In this paper we do not present a particular criterion to optimize them, since this depends on several factors such as the computational cost of evaluating the signal, the magnitude of the Fourier coefficients related to the frequencies to be computed, and the precision required in the results.

The method can present limitations if the signal has poor regularity, the frequencies are close to being resonant, or the amplitude of the target frequency is very small. Comparison with other methods must take into account the computational cost of the iterates, because high accuracy may require a large number of them. Indeed, if we want to compute frequencies up to a very high accuracy, then it is reasonable to use an arithmetic with a large number

of decimal digits, which, of course, significantly increases the computational cost of any iterate. As mentioned above, our approach also allows us to compute the amplitudes of the signal. However, if many amplitudes are required, then the use of collocation methods is most probably a better choice.

Finally, we want to emphasize that the "inverse problem" to the frequency analysis can also be tackled with the same ideas. Given a fixed $\omega \in \mathbb{R}^d$, it consists in computing an initial condition for an invariant torus of a Hamiltonian system with d degrees of freedom, or for a symplectic map in $\mathbb{R}^{2d}$, having ω as a vector of basic frequencies. Of course, ω must be Diophantine and we require a good enough approximation to this initial condition (assuming that the torus exists). The key is to combine the methodology of this paper for the frequency analysis (note that ω is the approximate frequency we use for the unfolding) with the computation of derivatives of frequencies with respect to parameters and initial conditions already introduced in [29]. This information allows us to refine the approximation for this initial condition by applying the Newton method to the d-dimensional frequency map. Note that the frequency map is well defined in a small neighborhood of a Diophantine torus, except for a set of exponentially small Lebesgue measure in the distance to the torus, and has $\mathcal{C}^\infty$-Whitney regularity. This problem is postponed to future work.

Appendix A. Some implementation details. In this appendix we discuss several implementation details in order to help the reader both obtain efficient algorithms to unfold a given quasi-periodic signal (section 2.3) and refine the computation of the target frequency (section 2.4). These comments can be extended mutatis mutandis to implement the method for computing Fourier coefficients (section 2.5).

In order to have explicit formulae for the extrapolation coefficients, we restrict our attention to the case when the number of iterates used for the extrapolation is a power of 2. As we pointed out after Definition 2.11, the key is that the values of L_j behave geometrically on j, so other choices can be made—and this may be even recommended depending on the problem. Let $\{S_L\}_{L\geq 1}$ be a sequence that behaves as in (23) (plus higher-order error terms). Then, we can approximate α by computing S_L for $p+1$ different values of L (behaving geometrically, not necessarily with an integer rate) and then solving a $(p+1)\times(p+1)$ linear system of equations.

Global parameters. In the following discussion p_u is the extrapolation order of the unfolding and $L = 2^{q_u}$ is the number of iterates used to compute any new iterate. As far as the computation of the frequency is concerned, p_r and $N = 2^{q_r}$ are the extrapolation order and the total number of unfolded iterates used to perform the refinement, respectively. As global variables, we precompute the following quantities:

- To perform the unfolding we compute the combinatorial numbers $\binom{L_j+k-1}{k}$ for $j = 0\dots p_u$ and $k = 1,\dots,p_u$, where $L_j = 2^{q_u-p_u+j}$. To refine the frequency we need $\binom{N_j+p_r}{p_r+1}$ for $j = 0,\dots,p_r$, where $N_j = 2^{q_r-p_r+j}$.
- We compute the extrapolation coefficients $c_j^{(m)}$ given by (20) both for the unfolding of the signal and the refinement of the frequency, that is, for $m = p_u-1$, $j = 0,\dots,p_u-1$, and for $m = p_r$, $j = 0,\dots,p_r$. To reduce the number of products in the evaluation of each unfolded iterate, we also introduce the scaled coefficients (see explanations

below):

$$\widetilde{c}_j^{(p_u-1)} = c_j^{(p_u-1)} \binom{L_j + p_u - 1}{p_u}^{-1}, \qquad j = 0, \dots, p_u - 1.$$

- To perform the full process we require the complex exponentials $\mathrm{e}^{\mathrm{i}m\omega_0}$ for $m = 0, \dots, 2^{q_u} + 2^{q_r} - 1$, where ω_0 is the approximation to the frequency. We do not precompute all these values but only the exponential $\mathrm{e}^{\mathrm{i}\omega_0}$. The remaining values are computed later by means of trigonometrical recurrences.

Unfolded iterates. Given a quasi-periodic sequence $\{z_n\}$ and an approximation ω_0 of one of the frequencies, let us describe an efficient way to implement the computation of the unfolded iterates of order p_u introduced in Definition 2.11. To compute each new iterate $z_n^{(2^{q_u},\omega_0,p_u)}$ we use $L = 2^{q_u}$ consecutive iterates z_l of the original signal for $l \in \{n, \dots, n + L - 1\}$. Since definition of $z_n^{(2^{q_u},\omega_0,p_u)}$ in (19) involves only the values of $\mathcal{Z}_n^{(L,\omega_0,p_u)}$ for $L = L_j$, with $j = 0, \dots, p_u - 1$, we can try to avoid the computation of $\mathcal{Z}_n^{(L,\omega_0,p_u)}$ for $L \neq L_j$. But note that if we use the definition of $\mathcal{Z}_n^{(L_j,\omega_0,p)}$ by the recursive sums in (17), then it involves the sum of $\mathcal{Z}_n^{(l,\omega_0,p-1)}$ for any $l = 1, \dots, L_j$. To compute the unfolded sequence $\{z_n^{(2^{q_u},\omega_0,p_u)}\}$, we proceed as follows:

- To compute the first unfolded iterate $z_1^{(2^q,\omega_0,p_u)}$, we compute the recursive sums $\mathcal{Z}_1^{(L_j,\omega_0,k)}$ for any $j = 0, \dots, p_u - 1$ and $k = 1, \dots, p_u$ by using the recurrences in (17) directly (i.e., by computing $\mathcal{Z}_1^{(l,\omega_0,k)}$ for any $l = 1, \dots, 2^{q_u}$ and $k = 1, \dots, p_u$).
- Assume that for some $n \geq 1$ we know $\mathcal{Z}_n^{(L_j,\omega_0,k)}$ for any $j = 0, \dots, p_u - 1$ and $k = 1, \dots, p_u$. Then, to obtain $\mathcal{Z}_{n+1}^{(L_j,\omega_0,k)}$ we do not have to compute the full recursive sums involved in (17); we just have to update the previous n-ones as follows:[6]

$$\begin{aligned}
\mathcal{Z}_{n+1}^{(L,\omega_0,1)} &= \mathcal{Z}_n^{(L,\omega_0,1)} + z_{L+n}\mathrm{e}^{-\mathrm{i}(L+n)\omega_0} - z_n\mathrm{e}^{-\mathrm{i}n\omega_0}, \\
\mathcal{Z}_{n+1}^{(L,\omega_0,k)} &= \mathcal{Z}_n^{(L,\omega_0,k)} + \mathcal{Z}_{n+1}^{(L,\omega_0,k-1)} - \binom{L+k-2}{k-1} z_n\mathrm{e}^{-\mathrm{i}n\omega_0}, \qquad k = 2, \dots, p_u.
\end{aligned}$$

- Once the recursive sums $\mathcal{Z}_n^{(L_j,\omega_0,p_u)}$ have been computed for any $j = 0, \dots, p_u - 1$, then we also avoid the computation of the averaged sums $\widetilde{\mathcal{Z}}_n^{(L_j,\omega_0,p_u)}$ by simply using the alternative formula

$$z_n^{(2^q,\omega_0,p_u)} = \left(\sum_{j=0}^{p_u-1} \widetilde{c}_j^{(p_u-1)} \mathcal{Z}_n^{(L_j,\omega_0,p_u)} \right) \mathrm{e}^{\mathrm{i}n\omega_0}.$$

Refinement of the frequency. To compute a refinement of the target frequency, using the unfolded signal obtained from the previous algorithm, we have to evaluate the lift of the projection of the iterates on the circle. We compute $x_n = \arg(z_n^{(2^{q_u},\omega_0,p_u)})$, taking suitable determinations of the argument so that x_n is an increasing function of n. Using the values of x_n for $n = 1, \dots, 2^{p_r}$, we compute the recursive sums $S_{N_j}^{(m)}$, introduced in Definition 2.13,

[6] Observe that these formulae perform especially quickly (in a computer) for $p_u = 2$, since then $\binom{L+p_u-2}{p_u-1} = L$ and we work with values of L that are powers of two. Products by 2 correspond to shifts using binary arithmetic.

for $m = 0, \ldots, p_r$ and $j = 0, \ldots, p_r$, and then the corresponding averaged ones, $\widetilde{S}_{N_j}^{(m)}$. The computation of these recursive sums is straightforward using the recurrent formulae, and it requires only storing in memory a matrix array of $(p_r + 1) \times (p_r + 1)$ elements. Then, the target frequency, say, $\omega_1 \simeq \omega_0$, is approximated as

$$\omega_1 \approx \Theta^{(p_r,q_r)} = \sum_{j=0}^{p_r} c_j^{(p_r)} \widetilde{S}_{N_j}^{(p_r)}.$$

Let us take the following into consideration:

- According Proposition 2.14, the error $e^{(p_r,q_r)}$ in the determination of ω_1 by $\Theta^{(p_r,q_r)}$ behaves like $|e^{(p_r,q_r)}| \approx C_{p_r} 2^{-(p_r+1)q_r}$. Then, we can try to estimate the value of C_{p_r} by means of two extrapolated values of order p_r, say, $\Theta^{(p_r,q_r)}$ and $\Theta^{(p_r,q_r-1)}$. As we expect $\Theta^{(p_r,q_r)}$ to be closer to ω_1 than $\Theta^{(p_r,q_r-1)}$, we estimate C_{p_r} by considering formula (28) for $q_r - 1$ and then replacing ω_1 by $\Theta^{(p_r,q_r)}$. We obtain the heuristic estimate (see [36])

$$|e^{(p_r,q_r)}| \approx 2^{-(p_r+1)} \nu |\Theta^{(p_r,q_r)} - \Theta^{(p_r,q_r-1)}|, \tag{42}$$

  where ν is a "safety parameter" to prevent the fact that C_{p_r} can oscillate as a function of q_r. In previous works we have used the value $\nu = 10$.
- Once the frequency ω_1 is known, formula (29) allows computing its Fourier coefficient, say, $\hat{\gamma}_{e_1}$, with high accuracy at a moderate cost. According to the notation of Proposition 2.18, we must take $k^* = e_1$ and $\omega^* = \omega_1$. We observe that we can estimate the committed error in the same way as for the frequency:

$$|e(k^*, p_f, q_f)| \approx 2^{-p_f} \nu |\Gamma^{(k^*,p_f,q_f)} - \Gamma^{(k^*,p_f,q_f-1)}|,$$

  where p_f and q_f are the extrapolation parameters selected to approximate $\hat{\gamma}_{e_1}$.
- The computation of, at least, a rough approximation to $\hat{\gamma}_{e_1}$ is highly recommended. As we pointed out in Remark 2.19, this is a simple test to ensure the correctness of the computed values ω_1.

Acknowledgments. We wish to acknowledge comments, suggestions, and fruitful discussions with Luis Benet, Àngel Jorba, Rafael de la Llave, and Carles Simó. We also thank À. Jorba for providing us with the initial condition (41).

REFERENCES

[1] V.I. Arnold, *Proof of a theorem of A. N. Kolmogorov on the invariance of quasi-periodic motions under small perturbations*, Russian Math. Surveys, 18 (1963), pp. 9–36.
[2] R. Barrio, *Performance of the Taylor series method for ODEs/DAEs*, Appl. Math. Comput., 163 (2005), pp. 525–545.
[3] H.W. Broer, G.B. Huitema, and M.B. Sevryuk, *Quasi-periodic Motions in Families of Dynamical Systems. Order amidst Chaos*, Lecture Notes in Math. 1645, Springer-Verlag, Berlin, 1996.
[4] H.W. Broer and M.B. Sevryuk, *KAM theory: Quasi-periodicity in dynamical systems*, in Handbook of Dynamical Systems, Vol. 3C, Elsevier, New York, 2010, pp. 249–344.
[5] A. Celletti and A. Giorgilli, *On the stability of the Lagrangian points in the spatial restricted problem of three bodies*, Celestial Mech. Dynam. Astronom., 50 (1991), pp. 31–58.

[6] R. de la Llave, *A tutorial on KAM theory*, in Smooth Ergodic Theory and Its Applications (Seattle, WA, 1999), Proc. Sympos. Pure Math. 69, AMS, Providence, RI, 2001, pp. 175–292.
[7] R. de la Llave, A. González, À. Jorba, and J. Villanueva, *KAM theory without action-angle variables*, Nonlinearity, 18 (2005), pp. 855–895.
[8] R. de la Llave and A. Luque, *Differentiability at the tip of Arnold tongues for Diophantine rotations: Numerical studies and renormalization group explanations*, J. Stat. Phys., 143 (2011), pp. 1154–1188.
[9] A. Delshams and P. Gutiérrez, *Estimates on invariant tori near an elliptic equilibrium point of a Hamiltonian system*, J. Differential Equations, 131 (1996), pp. 277–303.
[10] L.H. Eliasson, *Perturbations of stable invariant tori for Hamiltonian systems*, Ann. Scuola Norm. Sup. Pisa Cl. Sci. (4), 15 (1988), pp. 115–147.
[11] A. Giorgilli, A. Delshams, E. Fontich, L. Galgani, and C. Simó, *Effective stability for a Hamiltonian system near an elliptic equilibrium point, with an application to the restricted three-body problem*, J. Differential Equations, 77 (1989), pp. 167–198.
[12] G. Gómez, À. Jorba, C. Simó, and J. Masdemont, *Dynamics and Mission Design near Libration Points. Vol. IV. Advanced Methods for Triangular Points*, World Scientific Monograph Series in Mathematics 5, World Scientific, River Edge, NJ, 2001.
[13] G. Gómez, J.-M. Mondelo, and C. Simó, *A collocation method for the numerical Fourier analysis of quasi-periodic functions. I. Numerical tests and examples*, Discrete Contin. Dyn. Syst. Ser. B, 14 (2010), pp. 41–74.
[14] G. Gómez, J.-M. Mondelo, and C. Simó, *A collocation method for the numerical Fourier analysis of quasi-periodic functions. II. Analytical error estimates*, Discrete Contin. Dyn. Syst. Ser. B, 14 (2010), pp. 75–109.
[15] A. González, R. de la Llave, and A. Haro, *Singularity theory for non-twist KAM tori*, Mem. Amer. Math. Soc., to appear.
[16] M.R. Herman, *Une méthode pour minorer les exposants de Lyapounov et quelques exemples montrant le caractère local d'un théorème d'Arnol'd et de Moser sur le tore de dimension* 2, Comment. Math. Helv., 58 (1983), pp. 453–502.
[17] T.H. Jäger and J. Stark, *Towards a classification for quasiperiodically forced circle homeomorphisms*, J. London Math. Soc. (2), 73 (2006), pp. 727–744.
[18] W.B. Jones and V. Petersen, *Continued fractions and Szegő polynomials in frequency analysis and related topics*, in Proceedings of the International Conference on Rational Approximation, ICRA99 (Antwerp), Vol. 61, 2000, pp. 149–174.
[19] À. Jorba, *A numerical study on the existence of stable motions near the triangular points of the real earth-moon system*, Astronomy Astrophys., 364 (2000), pp. 327–338.
[20] À. Jorba and E. Olmedo, *On the computation of reducible invariant tori on a parallel computer*, SIAM J. Appl. Dyn. Syst., 8 (2009), pp. 1382–1404.
[21] À. Jorba, R. Ramírez-Ros, and J. Villanueva, *Effective reducibility of quasi-periodic linear equations close to constant coefficients*, SIAM J. Math. Anal., 28 (1997), pp. 178–188.
[22] À. Jorba and J. Villanueva, *On the normal behaviour of partially elliptic lower-dimensional tori of Hamiltonian systems*, Nonlinearity, 10 (1997), pp. 783–822.
[23] À. Jorba and J. Villanueva, *On the persistence of lower-dimensional invariant tori under quasi-periodic perturbations*, J. Nonlinear Sci., 7 (1997), pp. 427–473.
[24] À. Jorba and M. Zou, *A software package for the numerical integration of ODEs by means of high-order Taylor methods*, Experiment. Math., 14 (2005), pp. 99–117.
[25] J. Laskar, *The chaotic motion of the solar system. A numerical estimate of the size of the chaotic zones*, Icarus, 88 (1990), pp. 266–291.
[26] J. Laskar, *Introduction to frequency map analysis*, in Hamiltonian Systems with Three or More Degrees of Freedom (S'Agaró, 1995), NATO Adv. Sci. Inst. Ser. C Math. Phys. Sci. 533, Kluwer Academic Publishers, Dordrecht, The Netherlands, 1999, pp. 134–150.
[27] J. Laskar, *Frequency map analysis and quasiperiodic decompositions*, in Hamiltonian Systems and Fourier Analysis, Adv. Astron. Astrophys., Cambridge Scientific Publishers, Cambridge, UK, 2005, pp. 99–133.
[28] J. Laskar, C. Froeschlé, and A. Celletti, *The measure of chaos by the numerical analysis of the fundamental frequencies. Application to the standard mapping*, Phys. D, 56 (1992), pp. 253–269.

[29] A. Luque and J. Villanueva, *Computation of derivatives of the rotation number for parametric families of circle diffeomorphisms*, Phys. D, 237 (2008), pp. 2599–2615.
[30] A. Luque and J Villanueva, *Numerical computation of rotation numbers for quasi-periodic planar curves*, Phys. D, 238 (2009), pp. 2025–2044.
[31] A. Luque and J. Villanueva, *A KAM theorem without action-angle variables for elliptic lower dimensional tori*, Nonlinearity, 24 (2011), pp. 1033–1080.
[32] A.P. Markeev, *On the stability of the triangular libration points in the circular bounded three-body problem*, J. Appl. Math. Mech., 33 (1969), pp. 105–110.
[33] A.D. Perry and S. Wiggins, *KAM tori are very sticky: Rigorous lower bounds on the time to move away from an invariant Lagrangian torus with linear flow*, Phys. D, 71 (1994), pp. 102–121.
[34] R. McKenzie and V. Szebehely, *Non-linear stability motion around the triangular libration points*, Celestial Mechanics, 23 (1981), pp. 223–229.
[35] P. Robutel, F. Gabern, and A. Jorba, *The observed Trojans and the global dynamics around the Lagrangian points of the Sun-Jupiter system*, Celestial Mech. Dynam. Astronom., 92 (2005), pp. 53–69.
[36] T.M. Seara and J. Villanueva, *On the numerical computation of Diophantine rotation numbers of analytic circle maps*, Phys. D, 217 (2006), pp. 107–120.
[37] T.M. Seara and J. Villanueva, *Numerical computation of the asymptotic size of the rotation domain for the Arnold family*, Phys. D, 238 (2009), pp. 197–208.
[38] M.B. Sevryuk, *Invariant tori in quasi-periodic non-autonomous dynamical systems via Herman's method*, Discrete Contin. Dyn. Syst., 18 (2007), pp. 569–595.
[39] C. Simó, P. Sousa-Silva, and M. Terra, *Domains of Practical Stability near $l_{4,5}$ in the 3D Restricted Three-Body Problem*, in preparation.
[40] V. Szebehely, *Theory of Orbits: The Restricted Problem of Three Bodies*, Academic Press, New York, 1967.
[41] L.V. Vela-Arevalo and J.E. Marsden, *Time-frequency analysis of the restricted three-body problem: Transport and resonance transitions*, Classical Quantum Gravity, 21 (2004), pp. S351–S375.